Proceedings of the 2017 European School of High-Energy Physics, Evora, Portugal, 6–19 September 2017, edited by M. Mulders and G. Zanderighi, CERN Yellow Reports: School Proceedings, Vol. 3/2018, CERN-2018-006-SP (CERN, Geneva, 2018)

Lectures on QCD for hadron colliders

K. Melnikov
Institute for Theoretical Particle Physics, Karlsruhe Institute of Technology, Karlsruhe, Germany

Abstract
I discuss how perturbative QCD can be used to describe outcomes of hard hadron collisions in a detailed and precise way. To an extent that four lectures permit, we touch upon fixed order computations, resummations, parton distribution functions and parton showers. Main ideas behind these concepts are explained and derivations of many important results are given. The importance of understanding the soft and collinear limits of scattering amplitudes for the perturbative QCD description of hadron collisions is repeatedly emphasized.

Keywords
Lectures; QCD; perturbative computations; collider physics

1 Introduction

Experiments at the LHC where proton beams collide with the center of mass energy of 13 TeV are rightfully described as experiments at the energy frontier. Being at the energy frontier is important since, by increasing the collision energy, we create a situation where events with larger momentum transfer or larger energy deposition become possible. Such events are interesting because, if enough energy is packed into a small volume, it becomes possible to knock out new heavy elementary particles from the vacuum and to study their properties. It is hoped that, in doing so, we will be able to determine the Lagrangian that governs physics beyond the Standard Model.

This approach is at the heart of many measurements performed by ATLAS and CMS collaborations at the LHC. While these experiments scored clear successes since the start of the LHC in 2010, for example by discovering the celebrated Higgs boson [1, 2], they keep struggling to break through the "Standard Model barrier", see Fig. 1. As many exclusion limits improve to the point, that masses of new heavy particles, that are still not excluded, become so large that their frequent production at the LHC is hardly possible, it becomes clear that further searches for physics beyond the Standard Model based on the idea of clear, resonance-like structures emerging on top of relatively flat backgrounds will have to be supplemented by entirely new search strategies. Indeed, if new particles are not seen directly at the LHC, they can hide in complex final states, if they are light, or, if they are heavy, they can be virtually produced for short periods of time and then disappear back into the vacuum. In the latter case, we may hope to detect these virtual particles since they affect properties of Standard Model particles that we observe experimentally.

Given this situation, we are forced to think if precision physics at the LHC is possible and whether or not it can become a tool to discover physics beyond the Standard Model. It is important to realize that systematic precision studies at hadron colliders – aimed at discovering New Physics through indirect effects – were never attempted before. This is not surprising given the fact that hadrons are composite particles kept together by a poorly understood strong force. If we can not understand or compute properties of a single proton, how can we confidently describe what happens if two protons collide?

It is generally believed that this can be done if the collision energy is high enough and if we select events where momentum transfer is very large. Such events occur at small distances and, since physics of strong interactions at short distances becomes more perturbative, the understanding of the strong force improves. Of course, it never becomes perfect. So the question is how far we can drive the idea of the precision LHC physics before poor control over the strong force catches up with us.

https://doi.org/10.23730/CYRSP-2018-003.37

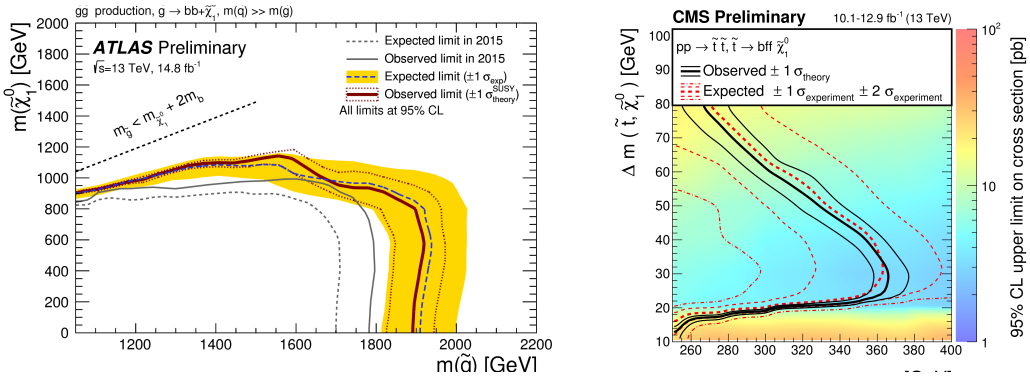

Fig. 1: Recent exclusion limits by ATLAS and CMS collaborations. The constraints on gluino and stop masses start challenging an established paradigm in high-energy physics.

This problem is non-trivial since, as we will see, we have very poor understanding of non-perturbative effects in hadron collisions. Unfortunately, non-perturbative effects need to be modeled anyhow, for instance to describe a transformation of partons to hadrons since it is the latter that interact with particle detectors. Since modeling non-perturbative effects necessarily involves some arbitrariness, it is important to find out which aspects of hadron collisions can be described and understood from first principles. This requirement is stronger than the ability of tools that we use to study hadron collisions (i.e. parton showers, fixed order computations, resummations etc.) to describe data since this can happen by accident or because one can tune these tools to do that.

As we will see in these lectures, all tools that we use to describe hadron collisions are based on approximations and all of them have limited range of applicability. For this reason, we need to understand, parametrically, the approximations that are made on the way from the Standard Model Lagrangian to a theory behind a particular measurement and we need to be convinced that a particular approximation is justified in each case. We need to be sure that the framework that we use is systematically improvable and, if not, we need to know its ultimate limit[1].

In short, we need to start asking questions about the foundations of what we do to describe hard hadron collisions and keep in mind that a significant fraction of the current lore, ideas and approaches dates back to times when even an order-of-magnitude understanding of hadron collider physics was considered a success. There is no question that currently we strive for more.

The key for describing hard scattering processes in hadron collisions is provided by the collinear factorization theorem in QCD [3]. Within this framework, colliding protons are viewed as beams of partons (massless quarks and gluons), each carrying a fraction of proton energy. Probabilities to find partons with definite energy fractions are called parton distribution functions (PDFs). These objects are universal, i.e. they do not depend on a process under investigation. Therefore, they can be determined in some processes and used to describe many other. Partons interact with each other and produce final states composed of Standard Model particles such a leptons, gauge bosons and QCD partons themselves. We interpret these QCD partons in final states as seeds of hadronic energy flows that are barely affected by non-perturbative QCD effects. We call these seeds jets.[2]

The production cross sections for processes with final states composed of QCD jets and Standard

[1] One of the possible questions is what is the order beyond which perturbative computations become *meaningless*?

[2] Unfortunately, due to time constraints, we could not discuss jets during the lectures. A comprehensive introduction into this very important subject can be found in Ref. [4].

Model particles in hard hadron collisions can thus be computed using the following formula

$$\mathrm{d}\sigma = \sum_{i_1,i_2} \int \mathrm{d}x_1 \mathrm{d}x_2 f_{i_1}(x_1) f_{i_2}(x_2) \mathrm{d}\sigma_{i_1 i_2}(x_1,x_2) F_J \left(1 + \mathcal{O}(\Lambda^n_{\mathrm{QCD}}/Q^n)\right), \quad n \geq 1. \tag{1}$$

Here $x_{1,2}$ are fractions of incoming hadron's energies carried by partons i_1 and i_2 and $f_{i_{1,2}}$ are the parton distribution functions. Finally, F_J is a function that, if necessary, defines jets by combining in a smart way QCD partons that appear in the final state.

The last term in Eq. (1) represents genuine non-perturbative effects that take us beyond the simple picture of parton scattering and fragmentation into jets. These effects are expected to be suppressed by the ratio of Λ_{QCD}/Q where Q is the smallest of hard scales in the problem and $\Lambda_{\mathrm{QCD}} \approx 300$ MeV is the non-perturbative parameter of QCD. Note that, according to Eq. (1) we *do not know how strongly* these effects are supposed to be suppressed. It is believed that, in many cases, the exponent n in Eq. (1) is $n = 2$ but there are arguments that suggest that $n = 1$ is possible especially if one studies complex kinematic distributions. Numerically, if $n = 1$ and $Q = 30$ GeV, the non-perturbative effects are estimated to be just a few percent. Note that non-perturbative of that magnitude are comparable to the accuracy to which partonic cross sections for certain hadron collider processes have been calculated. This implies that disentangling perturbative, non-perturbative and New Physics contributions to hadronic cross sections becomes problematic and may require careful investigation.

Note also that the non-perturbative contribution in Eq. (1) is highly non-trivial, in spite of its simple appearance since it contains different physical effects such as double-parton scattering, hadronization, contributions from the underlying events etc. Experimentalists know how important it is to simulate all these effects if one wants to extract real physics from hadron collisions but, according to the formula that we are going to use all the time, all these effects *are just power corrections* that can not be described from first principles. This fact alone should be worrisome enough since it shows a different take on what the LHC physics is all about by theorists and experimentalists. We will discuss how these two approaches can be reconciled when we will talk about the parton showers at the end of these lectures. Our next step is to discuss the basics of the quantum field theory of strong interactions, the QCD.

Before we dive into this discussion, let me state the obvious – it is impossible to explain the details of a complex quantum field theory, the QCD, and discuss its numerous applications to hadron collider physics in four lectures. Although I will do my best in communicating the main ideas of this theory, students should be well-advised to consult numerous textbooks on quantum field theory and the use of QCD to describe hadron collisions. An incomplete list of useful references can be found in the bibliography [5–9].

2 Basic facts about QCD for colliders

The upshot of the discussion in the previous Section and the collinear factorization formula Eq. (1) is that hard scattering processes at the LHC can be understood in terms of partons, i.e. quarks and gluons; only limited knowledge about protons is needed. Physics of quarks and gluons is governed by a field theory of strong interactions, the QCD. QCD is a non-abelian SU(3)-gauge theory so it is complicated and I can not describe all the details of this theory in these lectures. Instead, I will provide a few basic facts about QCD that we will use later. More information on QCD can be found in textbooks on particle physics and quantum field theory [5].

Similar to any other quantum field theory, QCD is described by a Lagrangian. It reads

$$\mathcal{L}_{\mathrm{QCD}} = \sum \bar{q}_j \left(i\hat{D} - m_j\right) q_j - \frac{1}{4} G^a_{\mu\nu} G^{a,\mu\nu}, \tag{2}$$

where we sum over six quark flavors – up, down, strange, charm, bottom and top. The theory describes interactions of these quarks with carriers of the strong force, the gluons. Quarks (gluons) transform under

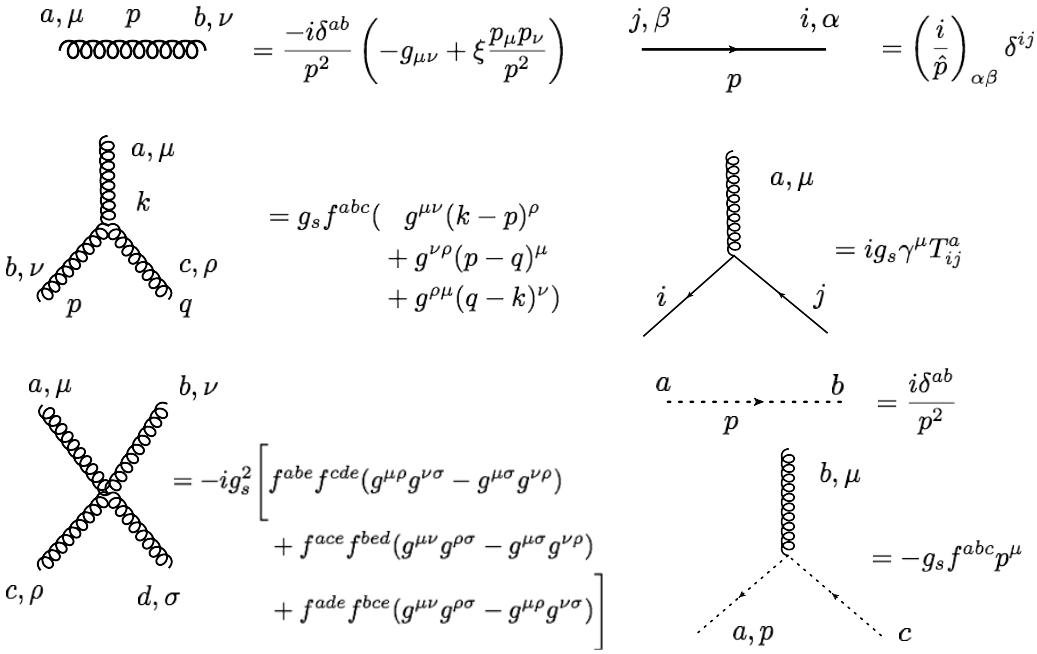

Fig. 2: QCD Feynman rules. Solid lines refer to quarks, wavy lines to gluons gluons and dashed lines to ghosts. Gluons in the three-gluon vertex are outgoing.

the fundamental (adjoined) representation of the gauge group SU(3), respectively. It is often said that there are also *unphysical* ghost particles in QCD; we will say a few words about them below. The various quantities that appear in the Lagrangian Eq. (2) are

$$D_\mu = \partial_\mu - ig_s T^a A^a_\mu, \quad G^a_{\mu\nu} = \partial_\mu A^a_\nu - \partial_\nu A^a_\mu + g_s f^{abc} A^b_\mu A^c_\nu, \tag{3}$$

where T^a and f^{abc} are generators and structure constants of the Lie algebra of the gauge group $SU(3)$.

It follows from the Lagrangian $\mathcal{L}_{\rm QCD}$ that gluons interact with quarks and antiquarks and also with other gluons. We can associate these interactions with color charges of the corresponding particles; however, since there are eight Lie algebra generators and many structure constants, it becomes difficult to say what the color charges really are. Since we can not observe color, physical processes are sensitive to average color charges; those are provided by the corresponding Casimir invariants of a particular representation R $C_R = \sum T^a_R T^a_R$. These Casimir invariants evaluate to $C_F = 4/3$ and $C_A = 3$ for the fundamental and adjoined representations, respectively. The importance of these numbers is that they show that the color charge of a gluon is larger than the color charge of a quark. Physically, this means that gluons interact stronger and radiate more, leading to e.g. higher multiplicities in gluon-initiated jets as compared to quark-initiated.

Similar to any quantum field theory, QCD can be characterized by Feynman rules that describe elementary interactions between different particles in the theory. The Feynman rules are shown in Fig. 2. It is seen from Fig. (2) that, indeed quarks interact with gluons and gluons interact with quarks and gluons. Interaction between quarks and gluons is very much QED-like except for additional SU(3) matrices that describe the color chargers.

In addition to quarks and gluons there are additional particles – ghosts. Ghosts are described by scalar *anti-commuting* fields, directly violating the spin-statistics theorem. The reason ghosts are so strange is that they appear in the theory for technical reasons, i.e. as a tool to allow for the quantization

of QCD in covariant gauges where gluons are assigned *four* polarizations instead of two. When this is done in QED, two additional photon polarizations decouple from the theory automatically thanks to the so-called Ward identities. In QCD this does not happen and the primary role of a ghost is to ensure that contributions of unphysical gluon polarizations are removed from cross sections with on-shell gluons even if the latter are computed using unphysical density matrices.

If physical gluon polarizations are used to describe external states, ghosts do not appear as external particles. For a gluon that moves along the z direction with momentum k, the two physical polarizations are

$$k = (k_0, 0, 0, k_0), \quad \epsilon^+ = \frac{1}{\sqrt{2}}(0, 1, i, 0), \quad \epsilon^- = \frac{1}{\sqrt{2}}(0, 1, -i, 0). \tag{4}$$

Note that physical gluon polarizations satisfy the following transversality condition

$$k \cdot \epsilon^{\pm} = 0. \tag{5}$$

We will make use of this condition when discussing soft and collinear limits of real emission matrix elements.

The situation with internal gluons is somewhat more complex; one can, in principle, employ gluons with only physical polarizations (and the non-propagating color-electric field) to do loop computations, but this leads to additional complications. In practice, it is more convenient to use covariant gauges and ghosts for computing loop corrections to scattering amplitudes and Green's functions.

Fixed order computations in QCD employ an expansion in the strong coupling constant α_s. However, we do not know its numerical value since, thanks to confinement, we observe colorless states – hadrons – whereas α_s refers to interactions between color charges that we associate with quarks and gluons. To determine α_s, we measure it at high energies where description of final states in terms of jets produced by quarks and gluons becomes appropriate. For example, from studies of Z-boson decays, we know that $\alpha_s(M_z) \approx 0.12$. We also find that if we want to describe QCD processes at other energies, we can absorb significant part of quantum corrections into the "running", i.e. "energy"-dependent, coupling constant. In particular, we find that at higher energies or, more precisely, higher momentum transfers, quantum corrections can be described by using a *smaller* coupling constant. This phenomenon, known as asymptotic freedom, is described by the formula

$$\alpha_s(\mu) = \frac{1}{\beta_0 \ln \frac{\mu^2}{\Lambda^2_{\rm QCD}}}, \quad \beta_0 = \frac{33 - 2n_f}{12\pi} \approx 0.5|_{n_f=5}, \tag{6}$$

where n_f is the number of "active" quark flavors.[3]

Asymptotic freedom is central to our ability to describe hard scattering processes at the LHC in QCD perturbative theory since the smallness of the coupling constant is a pre-requisite for the success of perturbative description. Note that for typical LHC processes the strong coupling constant is small but not tiny. This implies that quite often QCD corrections need to be computed to higher orders to claim high precision. The technology for computing next-to-leading QCD corrections to many processes of interest was developed in mid 1990s [10, 11] and an important ingredient was added about ten years ago [12, 13]. Since then, the development of theoretical methods for next-to-next-to-leading order (NNLO) computations became of great interest to the community of theorists interested in precision LHC phenomenology. Very recently, we have seen the emergence of several key technologies for NNLO computations [14] and dramatic increase in the number of their applications to LHC physics [15].

The use of QCD to describe hard scattering processes at the LHC is intimately connected with the detailed understanding of how scattering amplitudes behave in the so-called soft and collinear limits. The soft limit corresponds to a situation where energy of an emitted gluon becomes small. The collinear

[3] An "active" quark is a quark whose mass is smaller than the scale μ.

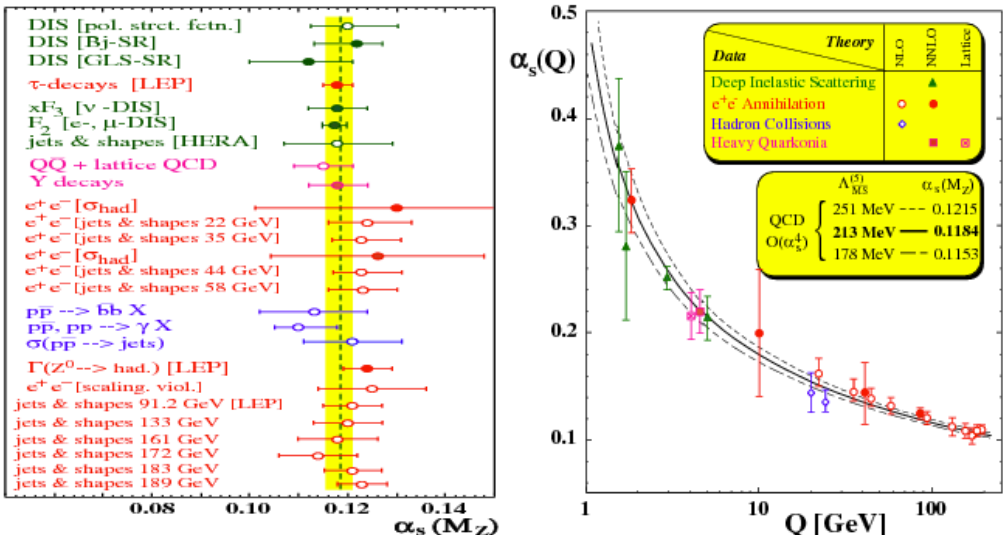

Fig. 3: The strong coupling constants as determined from different measurements and its evolution with momentum transfer.

limit corresponds to a situation where at least two external particles propagate in the same direction so that the relative angle between their momenta is small.

Scattering amplitudes become infinite if either soft or collinear limit is taken. Hence, soft and collinear limits describe kinematic situations where scattering amplitudes are large and which, therefore, provide dominant contributions to cross sections. This fact alone would have justified the need to understand soft and collinear limits of QCD amplitudes but there are more reasons to do that. They are listed below.

First, we can only apply perturbative QCD to describe observables that are *insensitive* to infra-red and collinear dynamics. This is because infra-red and collinear dynamics is non-perturbative and, therefore, it can not be described as an expansion in α_s. Hence, it is important to understand soft and collinear limits of scattering amplitudes to enable construction of observables that *can* be described and understood in perturbative QCD.

Second, soft and collinear limits of amplitudes lead to non-integrable singularities in perturbative computations of cross sections. Obtaining finite fixed order predictions in high orders of perturbative QCD requires us to understand in detail how soft and collinear singularities cancel in the total cross section or in other infra-red safe observables.

Third, soft and collinear limits often determine enhanced contributions to scattering amplitudes and cross sections. These enhanced contributions may invalidate fixed order predictions and, for this reason, they are essential for resummations, PDF evolution and parton showers. Understanding universal factorization properties of matrix elements in these limits is crucial for the success of the resummation program.

Finally, soft and collinear emissions dominate high-multiplicity final states. Understanding high-multiplicity final state in QCD is important for describing the evolution from hard scattering processes that occur at short distances to large distances where non-perturbative transition from QCD partons to observable hadrons occurs.

In what follows, we will look at different ways to describe hard hadron collisions, emphasizing the role of soft and collinear limits for these descriptions. We will start with a relatively simple picture of fixed order computations. We will continue by making it more complex in order to improve the description of certain observables. Quite often, I will use toy models and examples from QED to explain the

relevant physics, instead of talking about QCD directly. The reason for this is that QED physics is similar to QCD but QCD, being a non-abelian theory, is technically more involved. Therefore, understanding physics of hard collisions in a simpler gauge theory – QED – is a crucial step towards mastering QCD.

The remainder of these lectures is organized as follows. In the next Section I will discuss the production of lepton pairs in hadron collisions at leading order in perturbative expansion in QCD. We will find that the results of the calculation provide a decent description of rapidity and invariant mass distributions of a lepton pair but completely fail to describe its transverse momentum distribution. We will attempt to improve on this result by considering NLO QCD corrections to dilepton pair production in hadron collisions in Section 4. We will find that, although we can describe the transverse momentum distribution of a lepton pair at high $p_\perp$, we fail to do that at low values of the transverse momentum. In Section 5 we explain that at low values of the transverse momenta, perturbative expansion is in expansion in $\alpha_s \ln^2(s/p_\perp^2)$, rather than α_s, which can be of order one, so that all such contributions need to be resummed. We explain how to resum such terms in QCD perturbative series in Section 5. Upon doing so, we will discover that it is necessary to choose the factorization scale of parton distribution proportional to $p_\perp$, in order to achieve the resummation of $p_\perp$-dependent logarithms at small values of the transverse momentum. To understand the reason for that, we will discuss the parton distribution functions and the meaning of the factorization scale in Section 6. Parton distribution functions provide a limited information about the composition of the final state. To improve on that, parton showers are used. In Section 7 we explain the basic ideas behind parton showers and show how parton showers can be used to generate unweighted events. We conclude in Section 8.

3 Lepton pair production at leading order

In this Section, we discuss production of lepton pairs (e^+e^-, $\mu^+\mu^-$, $\tau^+\tau^-$) in hadron collisions at leading order in perturbative QCD. We will only consider the photon-mediated process; the exchange of the Z-boson between quarks and leptons will be neglected.

According to the factorization theorem Eq. (1), production of a lepton pair in hadron collisions is described by the following formula at leading order in perturbative QCD

$$\mathrm{d}\sigma_{H_1+H_2\to l^+l^-} = \sum_{i\in[q,\bar{q}]} \int \mathrm{d}x_1 \mathrm{d}x_2 f_i(x_1) f_{\bar{i}}(x_2)\, \mathrm{d}\sigma_{i\bar{i}\to l^+l^-}(x_1P_1, x_2P_2). \tag{7}$$

Here $P_{1,2}$ are the momenta of the colliding hadrons $H_{1,2}$, respectively. The momenta of incoming hadrons are taken to be light-like $P_1^2 = P_2^2 = 0$, i.e. all the mass effects are neglected. The four-momenta of the colliding massless quarks are then $p_1 = x_1P_1$ and $p_2 = x_2P_2$. Parton distribution functions $f_{q,\bar{q}}(x)$ are extracted from experimental measurements and are considered to be known for our purposes. Although there are gluon partons in a proton, they do not contribute to leading order cross section for lepton pair production.

To compute the hadronic cross section we need the cross section for the partonic process $q\bar{q} \to l^+l^-$. Computation of this cross section proceeds in a standard way. The matrix element reads

$$i\mathcal{M} = \frac{ie^2Q_q\delta_{km}}{Q^2}\left[\bar{u}(k_1,\lambda_1)\gamma_\mu v(k_2,\lambda_2)\right]\,\left[\bar{v}(p_2,\xi_2)\gamma^\mu u(p_1,\xi_1\right], \tag{8}$$

where Q_q is the electric charge of colliding quarks, k and m are their colors, $\lambda_{1,2}$ and $\xi_{1,2}$ are the polarization labels and $k_{1,2}$ are the four-momenta of a lepton and an anti-lepton, respectively. We will treat leptons as massless particles. We also introduced the four-momentum $Q = p_1 + p_2 = k_1 + k_2$ that flows through the propagator of a virtual photon.

To compute the cross section, we need to square the matrix element in Eq. (8) and sum it over polarizations of the initial and final state particles. This computation is simplified if we use the standard

trick that allows us to turn sums over polarizations into traces of products of Dirac matrices. The key formula reads

$$\sum_\lambda u(p,\lambda)_\alpha \bar{u}(p,\lambda)_\beta = \sum_\lambda v(p,\lambda)_\alpha \bar{v}(p,\lambda)_\beta = \hat{p}_{\alpha\beta}. \tag{9}$$

We use Eq. (9) and write

$$\sum_{\{\lambda,\xi\}} \sum_{\text{color}} |\mathcal{M}|^2 = N_c \frac{\left(e^2 Q_q\right)^2}{Q^4} \text{Tr}\left[\hat{k}_1 \gamma_\mu \hat{k}_2 \gamma_\nu\right] \text{Tr}\left[\hat{p}_2 \gamma^\mu \hat{p}_1 \gamma^\nu\right], \tag{10}$$

where $N_c = 3$ is the number of colors. We calculate the two traces using the standard formula

$$\text{Tr}\left[\hat{a}\gamma_\mu \hat{b}\gamma_\nu\right] = 4\left(a_\mu b_\nu + a_\nu b_\mu - g_{\mu\nu} a\cdot b\right), \tag{11}$$

and find

$$\sum_{\{\lambda,\xi\}} \sum_{\text{color}} |\mathcal{M}|^2 = \frac{32 N_c \left(e^2 Q_q\right)^2}{Q^4} \left[(k_1 p_2)(k_2 p_1) + (k_1 p_1)(k_1 p_2)\right]. \tag{12}$$

To compute the cross section, we write

$$\text{d}\sigma_{q\bar{q}\to e^+e^-} = \frac{1}{2s}\frac{1}{4}\frac{1}{N_c^2} \sum_{\{\lambda,\xi\}} \sum_{\text{color}} |\mathcal{M}|^2 \quad [\text{d}k_1][\text{d}k_2](2\pi)^4 \delta^{(4)}(p_1 + p_2 - k_1 - k_2), \tag{13}$$

where the prefactors describe the flux factor $2s = 4p_1p_2$ and the averaging over spins and colors of the incoming quarks. We also introduced a convenient notation for the Lorentz-invariant phase space of a single particle with momentum p

$$[\text{d}p] = \frac{\text{d}^3 p}{(2\pi)^3 2p_0}. \tag{14}$$

We will now rewrite the phase-space in a way that will allow us to separate two processes – the production of a virtual photon with the total momentum $Q = k_1 + k_2$ and the decay of this virtual photon to a lepton pair. For $q\bar{q} \to l^+l^-$ process the procedure that we describe is perhaps an overkill, but it is useful to understand it since it can be very helpful in more complicated cases. To this end, we introduce an auxiliary vector Q and write

$$1 = \int \text{d}^4 Q \; \delta^{(4)}(Q - p_1 - p_2). \tag{15}$$

We insert this integral into the phase space and simplify it by separating integration over $Q^2 = M^2$

$$\begin{aligned}
&[\text{d}k_1][\text{d}k_2](2\pi)^4 \delta(p_1 + p_2 - k_1 - k_2) \\
&= [\text{d}k_1][\text{d}k_2](2\pi)^4 \delta(p_1 + p_2 - k_1 - k_2) \text{d}^4 Q \delta^{(4)}(Q - p_1 - p_2) \\
&= \text{d}M^2 \delta(M^2 - Q^2) \text{d}^4 Q \delta^{(4)}(Q - p_1 - p_2) [\text{d}k_1][\text{d}k_2](2\pi)^4 \delta(Q - k_1 - k_2) \\
&= \text{d}M^2 \delta(M^2 - s) \; [\text{d}k_1][\text{d}k_2](2\pi)^4 \delta(Q - k_1 - k_2)|_{Q = p_1 + p_2, Q^2 = M^2}.
\end{aligned} \tag{16}$$

This formula does what we wanted since it separates the production of a (virtual) particle with the mass $M^2 = s$ from its decay to a di-lepton final state.

To compute the cross section we need to integrate over lepton momenta. There are different ways to do that. Since, according to Eqs. (12,13,16)

$$\text{d}\sigma_{q\bar{q}\to e^+e^-} \sim \int [\text{d}k_1][\text{d}k_2] \delta(Q - k_1 - k_2) \; k_1^\mu k_2^\nu (p_{1,\mu} p_{2,\nu} + p_{1,\nu} p_{2,\mu}), \tag{17}$$

we need to understand how to compute the following tensor integral

$$\int [\mathrm{d}k_1][\mathrm{d}k_2](2\pi)^4\delta(Q-k_1-k_2)k_1^\mu k_2^\nu = I^{\mu\nu}. \tag{18}$$

This integral is a rank-two tensor; therefore, it can only depend on the metric tensor and a rank-two tensor constructed using the vector Q. Thus, we write

$$I^{\mu\nu} = I_1 Q^2 g^{\mu\nu} + I_2 Q^\mu Q^\nu. \tag{19}$$

To compute the form factors $I_{1,2}$, it is convenient to contract $I_{\mu\nu}$ with $g_{\mu\nu}$ and $Q_\mu Q_\nu$, compute the contracted integrals separately and solve the system of linear equations for the two form factors. To illustrate this procedure, consider $g_{\mu\nu}I^{\mu\nu}$. This integral reads

$$Q^2\,(4I_1+I_2) = \int [\mathrm{d}k_1][\mathrm{d}k_2](2\pi)^4\delta(Q-k_1-k_2)(k_1k_2). \tag{20}$$

We use $k_1k_2 = Q^2/2$ and find

$$8I_1+2I_2 = \int [\mathrm{d}k_1][\mathrm{d}k_2](2\pi)^4\delta(Q-k_1-k_2). \tag{21}$$

The integral on the right hand side is the two-particle phase space. To compute it, it is convenient to use the fact that it is Lorentz-invariant and choose a frame where $Q=(Q_0,\vec{0})$ with $Q_0=\sqrt{Q^2}$. The integral becomes

$$I_{\mathrm{Lips}} = \int [\mathrm{d}k_1][\mathrm{d}k_2](2\pi)^4\delta(Q-k_1-k_2) = \int [\mathrm{d}k_1][\mathrm{d}k_2](2\pi)^4\delta(Q_0-\omega_1-\omega_2)\delta^{(3)}(\vec{k}_1+\vec{k}_2). \tag{22}$$

The integration over $\vec{k}_2$ is used to eliminate the three-momentum conserving δ-function; the integration over the absolute value of $|k_1|$ is used to eliminate the energy-conserving δ-function. The remaining integration over directions of the three-momentum k_1 are unconstrained. Therefore, we obtain

$$I_{\mathrm{Lips}} = \frac{1}{8\pi}\int\frac{\mathrm{d}\Omega_1}{4\pi} = \frac{1}{8\pi}\int_0^\pi \frac{\mathrm{d}\theta\sin\theta}{2}\int_0^{2\pi}\frac{\mathrm{d}\phi}{2\pi} = \frac{1}{8\pi}. \tag{23}$$

A very similar computation can be performed for $Q_\mu Q_\nu I^{\mu\nu} = Q^4(I_1+I_2)$. In fact, since $Qk_1 = Qk_2 = Q^2/2$, the calculation is almost identical. Solving the two linear equations for I_1, I_2, we find

$$I^{\mu\nu} = \frac{1}{96\pi}\left(Q^2 g^{\mu\nu} + 2Q^\mu Q^\nu\right). \tag{24}$$

We employ Eq. (24) to compute the cross section for $q\bar{q}\to l^+l^-$ and use $N_c=3$, $p_1p_2 = Q^2/2 = s/2$ and $Qp_1 = Q^2/2 = s/2$, to arrive at the final result

$$\frac{\mathrm{d}\sigma_{q\bar{q}\to e^+e^-}}{\mathrm{d}M^2} = \frac{4\pi\alpha^2 Q_q^2}{9s}\,\delta(s-M^2). \tag{25}$$

We will use Eq. (25) to compute the hadronic cross section for lepton pair production. To this end, we employ the collinear factorization formula Eq. (7) and the partonic cross section Eq. (25), integrated over M^2, to obtain

$$\sigma_{H_1+H_2\to p_1+p_2} = \sum_{i\in[q,\bar{q}]}\int \mathrm{d}x_1\mathrm{d}x_2 f_i(x_1)f_{\bar{i}}(x_2)\,\frac{4\pi\alpha^2Q_i^2}{9M^2}. \tag{26}$$

Here the invariant mass of the lepton pair M^2 is expressed through the center of mass energy squared of the two colliding hadrons S as $M^2 = Sx_1x_2$.

It is convenient to rewrite the integration over x_1 and x_2 through the invariant mass M^2 and the *rapidity* of the lepton pair. The rapidity is defined as

$$Y = \frac{1}{2}\ln\frac{Q_0 + Q_z}{Q_0 - Q_z}, \tag{27}$$

where Q_z is the component of the four-momentum of the lepton pair $Q = k_1 + k_2$ along the collision axis. Using the momentum conservation $Q = k_1 + k_2 = p_1 + p_2 = x_1P_1 + x_2P_2$ and the fact that hadrons collide in the center-of-mass frame along the z-axis, we find

$$Y = \frac{1}{2}\ln\frac{Q_0 + Q_z}{Q_0 - Q_z} = \frac{1}{2}\ln\frac{P_2Q}{P_1Q} = \frac{1}{2}\ln\frac{x_1}{x_2}\frac{p_2Q}{p_1Q} = \frac{1}{2}\ln\frac{x_1}{x_2}. \tag{28}$$

Since $M^2 = Sx_1x_2$ we can write

$$x_1 = \sqrt{\frac{M^2}{S}}e^{Y}, \quad x_2 = \sqrt{\frac{M^2}{S}}e^{-Y}. \tag{29}$$

Finally, we can trade the integration over x_1, x_2 for the integration over M^2 and Y. Computing the Jacobian of the transformation, we obtain

$$\mathrm{d}x_1\mathrm{d}x_2 = \frac{\mathrm{d}M^2\mathrm{d}Y}{S}. \tag{30}$$

Integration boundaries follow from the conditions on the momenta fractions $0 < x_{1,2} < 1$ and read

$$|Y| < \frac{1}{2}\ln\frac{S}{M^2}, \quad 0 < M^2 < S. \tag{31}$$

The final result for the hadronic cross-section reads

$$\frac{M^2\,\mathrm{d}\sigma_{H_1+H_2\to l^+l^-}}{\mathrm{d}M^2\mathrm{d}Y} = \frac{4\pi\alpha^2}{9S}\sum_{i\in[q,\bar{q}]}Q_i^2 f_i(x_1^*)f_{\bar{i}}(x_2^*), \tag{32}$$

where $x_{1,2}^* = \sqrt{M^2/S}e^{\pm Y}$.

The above formula provides interesting information about kinematics of lepton pairs that are produced in hadron collisions. It predicts non-trivial distributions in the invariant mass and the rapidity of a lepton pair. However, the very same formula also predicts that momenta of lepton pairs are aligned with the collision axis and that no lepton pairs with non-vanishing momenta components transverse to the collision axis are produced in hadron collisions. Indeed, since $Q = x_1P_1 + x_2P_2$, the transverse momentum distribution predicted by our computation reads $\mathrm{d}\sigma/\mathrm{d}^2\vec{Q}_\perp \sim \delta(\vec{Q}_\perp)$.

It is instructive to compare these predictions with the results of actual measurements. The measured distributions of the invariant masses of lepton pairs and the rapidity are shown in Fig. 4. The experimental results include the Z exchange between quarks and leptons, c.f. the peak in the left pane at around $M_{ll} \sim 90$ Gev, so they can not be directly compared with our computation. However, if we were to include the Z-exchange into our theoretical prediction, we would describe data shown in Fig. 4 reasonably well.

However, the situation becomes very different for the transverse momentum distribution of a lepton pair, shown in Fig. 5. As we explained earlier, the leading order computation predicts that lepton

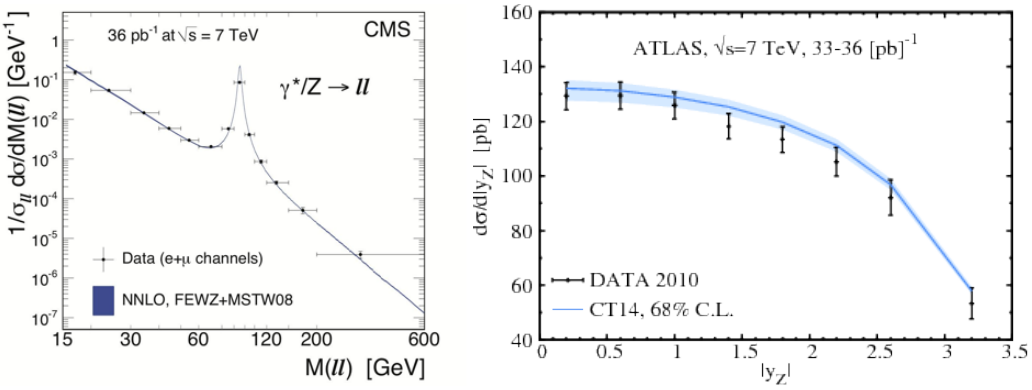

Fig. 4: Invariant mass (left) and rapidity (right) distributions of lepton pairs at the LHC. Z-exchanges are included and the results compared with theoretical predictions that include higher order QCD corrections. If we were to include the Z-exchange in our cross section computation and then plot the invariant mass and the rapidity distributions, we would describe experimental data reasonably well.

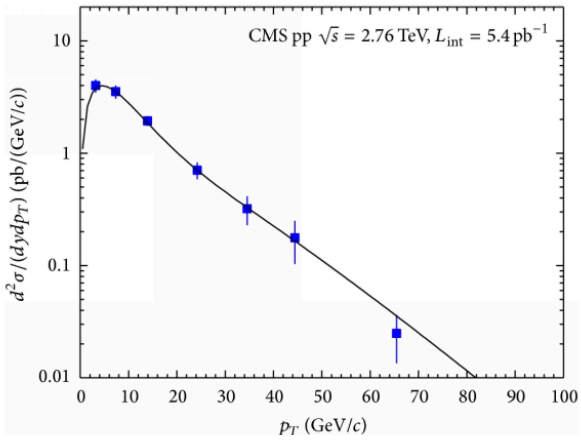

Fig. 5: The lepton pair transverse momentum distribution measured by the CMS collaboration. Clearly, it is very different from $\mathrm{d}\sigma/\mathrm{d}^2 p_\perp \sim \delta^{(2)}(\vec{p}_\perp)$ predicted by the leading order computation.

pairs produced in hadron collisions have vanishing transverse momenta. This prediction is in *direct contradiction* with the results of experimental measurements shown in Fig. 5. To summarize, we see that leading order QCD theory works reasonably well for the invariant mass and the rapidity distributions but that it fails for the transverse momentum distribution of a lepton pair. So, what is going on?

To understand how non-trivial transverse momentum distribution of a lepton pair can be produced, we recall that our computation of the lepton pair production cross section was performed at leading order in perturbative QCD. If we go to higher orders, two things can happen. First, the interaction strengths between quarks and photons changes because of the *virtual* QCD corrections. Second, a gluon can be emitted by an incoming quark or an incoming anti-quark; such contributions are called *real-emission* corrections. If this gluon happens to have a non-vanishing transverse momentum, the lepton pair will have to balance it because of momentum conservation; this may generate a continuous spectrum of lepton pairs with different transverse momenta in accord with experimental measurements. We will substantiate these considerations with mathematical formulas in the next Section.

4 Lepton pair production at next-to-leading order in perturbative QCD

To make this discussion more quantitative, we need to be able to compute next-to-leading order QCD corrections to lepton pair production cross section in hadron collisions. We will start with the discussion of the real emission process $q\bar{q} \to e^+e^- + g$. We will denote the gluon momentum as p_3. We write the real-emission cross section in a particular way

$$\mathrm{d}\sigma_R = \frac{1}{2s}\int [\mathrm{d}p_3] F_{\mathrm{LM}}(1,2,3), \tag{33}$$

where

$$F_{\mathrm{LM}}(1,2,3) = N_A \overline{|M(1,2,3)|}^2 (2\pi)^4 \delta(p_1+p_2-p_3-k_1-k_2)\ \mathrm{dLips}_{e^+e^-}, \tag{34}$$

N_A is the required symmetry factor that includes averaging over spins and colors of the colliding partons and $\overline{|(M(1,2,3)|}^2$ is the matrix element squared for $q\bar{q} \to e^+e^- + g$ process, summed over polarizations and colors of all particles. Also, $\mathrm{dLips}_{e^+e^-} = [\mathrm{d}k_1][\mathrm{d}k_2]$ is the phase-space of the lepton pair. Note also that observables are reconstructed from the momenta of particles that appear in the function F_{LM}; this remark will be important once we get to the discussion of the *subtraction procedure* later in this Section.

We would like to compute the contribution of the the real-emission process to the production rate of lepton pairs in hadron collisions. This requires integrating over gluon and dilepton phase spaces in Eq. (33). We will show now that this integral *can not be computed*.

To see this, let us understand the conditions on the matrix elements that ensure that the real emission contribution can be computed. We begin by considering the integration over gluon energy. The phase space element scales as

$$[\mathrm{d}p_3] \sim \frac{E_3^2 \mathrm{d}E_3}{E_3} \sim E_3 \mathrm{d}E_3. \tag{35}$$

The lower integration boundary is $E_3 = 0$, the upper integration boundary follows from the energy conservation. Therefore

$$\mathrm{d}\sigma_R \sim \int\limits_0^{E_3^{\mathrm{max}}} \mathrm{d}E_3 E_3 |\mathcal{M}(1,2,3)|^2. \tag{36}$$

It follows that if $\lim_{E_3\to 0} M(1,2,3) \sim E_3^{-1}$, the integral over E_3 does not converge at the lower integration boundary.

We can check how the matrix element behaves when the energy of the gluon becomes small. The matrix element reads

$$\mathcal{M}(1,2,3) = g_s T^a_{ji} \bar{v}(p_2) \left[\frac{\gamma^\mu (\hat{p}_1 - \hat{p}_3)\hat{\epsilon}}{(p_1-p_3)^2} - \frac{\hat{\epsilon}\,(\hat{p}_2-\hat{p}_3)\,\gamma^\mu}{(p_2-p_3)^2} \right] u(p_1) \times \frac{[e^2 Q_q]}{Q^2} \bar{u}(k_1)\gamma_\mu v(k_2), \tag{37}$$

where, as before, Q is the four-momentum of the lepton pair, g_s is the strong coupling constant and ϵ^μ is the gluon polarization vector.

We are interested in the behavior of the amplitude Eq. (37) in the limit $E_3 \to 0$; this implies that p_3 vanishes, component by component. Since $(p_{1,2}-p_3)^2 = -2p_{1,2}p_3 \sim O(E_3)$ and since we are only interested in the contribution to $\mathcal{M}$ that scales as E_3^{-1}, we can neglect p_3 in the numerators of the two terms in square brackets in Eq. (37) and keep it in the denominators.

Further simplifications are possible in Eq. (37). Consider the first term in square brackets as an example. We find

$$\bar{v}(p_2) \left[\frac{\gamma^\mu (\hat{p}_1 - \hat{p}_3)\hat{\epsilon}}{(p_1-p_3)^2} \right] u(p_1) \to \frac{\bar{v}(p_2)\gamma^\mu \hat{p}_1 \hat{\epsilon} u(p_1)}{(-2p_1p_3)} \to -\frac{p_1\cdot\epsilon}{p_1\cdot p_3}\,\bar{v}(p_2)\gamma^\mu u(p_1), \tag{38}$$

where we used $\hat{p}_1\hat{\epsilon}u(p_1) = (2p_1\cdot\epsilon - \hat{\epsilon}\hat{p}_1)u(p_1) = 2p_1\cdot\epsilon u(p_1)$ as follows from the anticommutation relations of the Dirac matrices and the Dirac equation $\hat{p}_1 u(p_1) = 0$.

Repeating the calculation to simplify the second term in the square brackets in Eq. (37), we find the soft limit of the amplitude

$$\lim_{E_3\to 0}\mathcal{M}(1,2,3) = -g_s T^a_{ij}\left(\frac{p_1\epsilon}{p_1p_3} - \frac{p_2\epsilon}{p_2p_3}\right)\mathcal{M}'(1,2). \tag{39}$$

Here $\mathcal{M}'(1,2)$ is the amplitude for the elastic process $q\bar{q}\to e^+e^-$ with the color factor δ_{ij} removed. It is now straightforward to compute the amplitude squared summed over colors and polarizations. We obtain

$$\lim_{E_3\to 0}|\mathcal{M}(1,2,3)|^2 = \mathrm{Eik}(1,2,3)|\mathcal{M}(1,2)|^2, \tag{40}$$

where the eikonal factor reads

$$\mathrm{Eik}(1,2,3) = g_s^2 C_F\frac{2p_1p_2}{(p_1p_3)(p_2p_3)}. \tag{41}$$

There are two comments to make about this result. First, soft limits of scattering amplitudes are *universal*; they depend on the color charges of colliding energetic particles and their momenta. The hard scattering amplitude that appears in the soft limit describes a process without soft gluon radiation, i.e. $q\bar{q}\to e^+e^-$ in our case. Second, it is clear from Eqs. (40,41) that the amplitude squared for the $q\bar{q}\to e^+e^- + g$ process indeed scales as E_3^{-2} in the soft limit. As the result, its contribution to the real emission cross section diverges at $E_3 = 0$

$$\sigma_R \sim \int_0^{E_{\rm max}}\frac{\mathrm{d}E_3}{E_3} = \infty, \tag{42}$$

and, therefore, can not be computed.

We will discuss how to solve this problem below. For now, we will study another kinematic region where integration over the gluon four-momentum becomes problematic. To appreciate that there might be another problem, consider again the gluon emission amplitude shown in Eq. (37) and look at the first term in square brackets that describes gluon emission off the incoming quark. The denominator of this term is $s_{13} = (p_1 - p_3)^2 = -2p_1p_3 = -2E_1E_3(1-\cos\theta_{13})$. It vanishes if the energy of the emitted gluon vanishes – this is the situation that we just discussed. However, s_{13} also vanishes if $\theta_{13}\to 0$ that corresponds to a situation when the gluon is emitted along the direction of the incoming quark. Since the gluon emission phase space scales as $[\mathrm{d}p_3]\sim\theta_{13}\mathrm{d}\theta_{13}$, for small θ_{13} the amplitude squared should diverge weaker than $|\mathcal{M}(1,2,3)|^2\sim\theta_{13}^{-2}$ for the rate to be calculable. Unfortunately, a naive computation of this *collinear* limit

$$|\mathcal{M}(1,2,3)|^2\sim s_{13}^{-2}\sim\theta_{13}^{-4}, \tag{43}$$

indicates a very strong singularity which, however, is inconsistent with e.g. the soft limit of the amplitude squared, c.f. Eq. (41).

To understand what is going on, we need to study the collinear limit of the amplitude more carefully. To this end, it is convenient to employ the so-called Sudakov decomposition for the gluon momentum

$$p_3 = xp_1 + \beta p_2 + p_{3\perp}, \tag{44}$$

where the transverse momentum is defined by the conditions $p_1p_{3\perp} = p_2p_{3\perp} = 0$. Since the gluon p_3 is on the mass shell, $p_3^2 = 0$, we find

$$sx\beta = \vec{p}_{3,\perp}^{\,2}. \tag{45}$$

If the gluon is emitted along the direction of the incoming quark, $x \sim 1$, $p_{3,\perp} \sim \sqrt{s}\theta_{13}$ and $\beta \sim \theta_{13}^2$; the latter scaling follows from Eq. (45).

We use the Sudakov decomposition in the matrix element for $q\bar{q} \to e^+e^- + g$ assuming that the gluon is emitted collinearly to the momentum of the incoming quark. We will first show that the singularity that appears when $\theta_{13} \to 0$ is *significantly weaker* than the naive estimate Eq. (43). To see this, consider the most singular contribution to the amplitude in the $\theta_{13} \to 0$ limit that arises from the term that describes gluon emission off the quark line

$$\mathcal{M}_q(1,2,3) = g_s T^a_{ji} \bar{v}(p_2) \left[\frac{\gamma^\mu(\hat{p}_1 - \hat{p}_3)\hat{\epsilon}}{-2p_1p_3}\right] u(p_1) \times \frac{[e^2Q_q]}{Q^2}\bar{u}(k_1)\gamma_\mu v(k_2). \tag{46}$$

We use the Sudakov decomposition for the gluon momentum in this expression and look for the most singular term in the limit $\theta_{13} \to 0$. We replace p_3 using the Sudakov decomposition as in Eq. (44) and use scalings of β and $p_{3,\perp}$ with θ_{13} to discard subleading terms. The most singular term corresponds to the amplitude Eq. (46) with p_3 in the numerator replaced with xp_1. We find

$$\begin{aligned}\lim_{\theta_{13}\to 0} \mathcal{M}_q(1,2,3) &= -\frac{g_s T^a_{ij}}{2p_1p_3}(1-x)\bar{v}(p_2)\gamma^\mu \hat{p}_1 \epsilon u(p_1) \times \frac{[e^2Q_q]}{Q^2}\bar{u}(k_1)\gamma_\mu v(k_2) \\ &= -\frac{g_s T^a_{ij}}{2p_1p_3}(1-x)(2p_1\epsilon)\ \bar{v}(p_2)\gamma^\mu u(p_1) \times \frac{[e^2Q_q]}{Q^2}\bar{u}(k_1)\gamma_\mu v(k_2),\end{aligned} \tag{47}$$

where again at the last step we used the anti-commutation relation of the Dirac matrices and the Dirac equation $\hat{p}_1 u(p_1) = 0$.

The expression Eq. (47) seems to confirm the naive estimate of the strength of the singularity of the amplitude in the $\theta_{13} \to 0$ limit since $p_1p_3 \sim \beta \sim \theta_{13}^2$ and the numerator in Eq. (47) contains no θ_{13}. However this conclusion is misleading. Indeed, since ϵ is the polarization vector of a physical gluon, it satisfies the transversality condition $p_3\epsilon = 0$. We use this equation to find the scaling of the scalar product $p_1\epsilon$ that appears in in Eq.(47) using the Sudakov decomposition for p_3. We obtain $x(p_1\epsilon) + \beta(p_2\epsilon) + (p_{3\perp}\epsilon) = 0$, so that

$$p_1\epsilon = -\frac{p_{3\perp}\epsilon}{x} - \frac{\beta p_2\epsilon}{x} \sim \mathcal{O}(\theta_{13}). \tag{48}$$

Hence, thanks to the fact that we deal with the gauge theory, the matrix element in the collinear limit is less singular than the naive estimate shows. Using Eqs. (47,48), we find $\mathcal{M}(1,2,3) \sim \theta_{13}^{-1}$.

To compute the collinear limit of the amplitude, we need to account for all terms that scale as θ_{13}^{-1} but all other terms can be neglected. In particular, we do not need to consider contributions to the amplitude which describe the emission of gluons by an anti-quark since they scale as $\mathcal{O}(1)$. The calculation is straightforward but somewhat messy and we do not present it here. Instead, we just report the result

$$\lim_{\theta_{13}\to 0} \overline{|\mathcal{M}(1,2,3)|}^2 = \frac{2g_s^2}{(p_1-p_3)^2} P_{qq}\left(\frac{E_1}{E_1-E_3}\right) \overline{|\mathcal{M}(1-3,2)|}^2, \tag{49}$$

where

$$P_{qq} = C_F \frac{1+z^2}{1-z} \tag{50}$$

is the so-called $q \to qg$ splitting function and the notation $\mathcal{M}(1-3,2)$ means that the matrix element for the leading order process $q\bar{q} \to e^+e^-$ has to be computed for the four-momenta of the incoming quark given by $p_q^\mu = (E_1 - E_3)/E_1\ p_1^\mu$. Clearly, p_q can be thought of as the four-momentum of a quark *after* it emitted the collinear gluon with the energy E_3.

It should be clear from this discussion that a very similar situation occurs when the gluon is emitted by an incoming anti-quark. The limit for the amplitude squared in this case is obtained after simple modifications in Eq. (49)

$$\lim_{\theta_{23}\to 0} \overline{|\mathcal{M}(1,2,3)|}^2 = \frac{2g_s^2}{(p_2-p_3)^2} P_{qq}\left(\frac{E_2}{E_2-E_3}\right) \overline{|\mathcal{M}(1,2-3)|}^2, \tag{51}$$

where $\mathcal{M}(1,2-3)$ refers to leading order matrix element where the four-momentum of an anti-quark is taken to be $p_{\bar{q}}^\mu = (E_2-E_3)/E_2\, p_2^\mu$.

Clearly, since the matrix element squared scales as $|\mathcal{M}(1,2,3)|^2 \sim \theta^{-2}$ for small emission angles, it is not possible to compute the contribution of the real emission process to the production rate

$$\sigma_R \sim \int [\mathrm{d}p_3] |\mathcal{M}(1,2,3)|^2 \sim \int_0^\pi \theta \mathrm{d}\theta\, \theta^{-2} = \infty. \tag{52}$$

To understand what to do with these infinities, we need to turn them into something tractable. To this end, we use an idea of the *regularization* that appears in theoretical physics over and again. It is based on the understanding that all infinities look *similar* and so it is difficult to trace where they come from. On the other hand, if we introduce a parameter that allows us to control how these infinities arise in the corresponding limits, we can start to distinguish between them thereby making the first step towards understanding what to do about them.

There are different ways to regularize these infinities. One option is to imagine that the scattering process occurs in a space-time whose dimensionality is *larger* than four. Scalings of amplitudes in the soft and collinear limits remain the same but the scaling of the gluon phase space changes. Indeed, if we consider, for the sake of example, the process $q\bar{q} \to e^+e^- + g$ in the five-dimensional space-time, we find

$$[\mathrm{d}p_3]_{5d} \sim E_3^2 \mathrm{d}E_3, \quad [\mathrm{d}p_3]_{5d} \sim \theta^2 \mathrm{d}\theta. \tag{53}$$

These scalings of the phase space imply that soft and collinear limits of the amplitude squared can be integrated in five-dimensional space-time without a problem. Of course at this point it is not clear how this observation can be used to perform computations in four-dimensional space-time since four- and five-dimensional space-times are clearly rather different.

An interesting idea [16] is to treat the dimensionality of space-time as a formal parameter *without* assuming it to be integer. It is conventional to denote the space-time dimensionality as d and to write $d = 4-2\epsilon$. If we are able to perform all the relevant computations without requiring d to be integer and if, at the end, we can take the $\epsilon \to 0$ limit, we will be able to write our results as an expansion around four-dimensional space-time and regularize infinities that we observed earlier.

It is easy to see that this strategy is quite sensible. Indeed, the phase-space element for a massless particle with four momentum $k = (k_0, \vec{k})$, $k^2 = 0$ in a d-dimensional space-time is defined as

$$[\mathrm{d}k] = \frac{k_0^{d-2} \mathrm{d}k_0 \mathrm{d}\Omega^{(d-1)}}{2(2\pi)^{d-1}}. \tag{54}$$

The solid angle in non-integer number of dimensions is defined recursively

$$\mathrm{d}\Omega^{(d-1)} = \mathrm{d}\cos\theta\, (1-\cos^2\theta)^{(d-4)/2}\, \mathrm{d}\Omega^{(d-2)}, \qquad \Omega^{(d)} = \frac{2\pi^{d/2}}{\Gamma(d/2)}. \tag{55}$$

We will now show that this modification of the phase-space regularizes soft and collinear singularities. To this end, consider the integral of the eikonal factor over the single gluon phase space. It reads

$$I_E = \int [\mathrm{d}p_3] \frac{2p_1\cdot p_2}{p_3\cdot p_1 p_3\cdot p_2} \theta(E_{\max} - E_3). \tag{56}$$

The momenta $p_{1,2}$ are back-to-back and we choose the z-axis to be the collision axis. The resulting integral becomes

$$\begin{aligned} I_E &= \int\limits_0^{E\text{max}} \frac{4E_3^{d-2}\text{d}E_3}{2(2\pi)^{d-1}E_3^3} \int\limits_{-1}^{1} \frac{\text{d}\cos\theta(1-\cos^2\theta)^{(d-4)/2}\,\text{d}\Omega^{(d-2)}}{(1-\cos^2\theta)} \\ &= \frac{2\Omega^{(d-2)}}{(2\pi)^{d-1}} \int\limits_0^{E_\text{max}} \frac{\text{d}E_3}{E_3^{1+2\epsilon}} \int\limits_{-1}^{1} \frac{\text{d}\cos\theta}{(1-\cos^2\theta)^{1+\epsilon}}. \end{aligned} \tag{57}$$

The last two integrals are easy to compute assuming that $\epsilon < 0$, so that integrals converge at the otherwise problematic boundaries. The integral over gluon energy is straightforward

$$\int\limits_0^{E\text{max}} \frac{\text{d}E_3}{E_3^{1+2\epsilon}} = -\frac{E_\text{max}^{-2\epsilon}}{2\epsilon}. \tag{58}$$

To compute the integral over the polar angle in Eq. (57) we need to change the integration variable $\cos\theta = 1-2x$, $0<x<1$. Then

$$\int\limits_{-1}^{1} \frac{\text{d}\cos\theta}{(1-\cos^2\theta)^{1+\epsilon}} = 2^{-1-2\epsilon}\int\limits_0^1 \text{d}x(x(1-x))^{-1-\epsilon} = -2^{-2\epsilon}\frac{\Gamma^2(1-\epsilon)}{\epsilon\Gamma(1-2\epsilon)}. \tag{59}$$

Since $\Gamma(1+x\epsilon)\approx 1+\mathcal{O}(\epsilon)$, we find

$$I_E = \frac{1}{4\pi^2\epsilon^2} + \mathcal{O}(1/\epsilon). \tag{60}$$

It follows from the above equation that that integrations over energy and the polar angle produce terms that become infinite in the $d\to 4$ limit. However, the relevant integrals are indeed regularized and we can study how the $1/\epsilon$ singularities disappear when all the different contributions to cross sections are combined.

We will try to achieve this *without* integrating over any measureable degrees of freedom of the emitted gluon. Since, as we saw, the $1/\epsilon$ singularities appear only after integration over gluon energies and angles, we need to design a procedure that allows us to integrate over emitted gluons *without* affecting the observables. This is accomplished with the help of the so-called so-called *subtraction* procedure. The idea is to systematically subtract simplified versions of real emission contributions that, on one hand, make the (subtracted) real emission cross sections integrable in $d=4$ and, on the other hand, are simple enough to be integrated over the unresolved phase-space in $d\neq 4$.

To see how this procedure works in detail, it is convenient to introduce particular notation to extract soft and collinear limits from the matrix elements and the corresponding phase space. We write

$$\begin{aligned} S_3\text{F}_\text{LM}(1,2,3) &= \lim_{p_3\to 0} F_\text{LM}(1,2,3) = g_s^2 C_F \frac{2p_1p_2}{(p_1p_3)(p_2p_3)} F_\text{LM}(1,2), \\ C_{31}F_\text{LM}(1,2,3) &= \lim_{\theta_{13}\to 0} F_\text{LM}(1,2,3) = \frac{2g_s^2}{(p_1-p_3)^2} P_{qq}\left(\frac{E_1}{E_1-E_3}\right) F_\text{LM}(1-3,2), \\ C_{32}F_\text{LM}(1,2,3) &= \lim_{\theta_{23}\to 0} F_\text{LM}(1,2,3) = \frac{2g_s^2}{(p_2-p_3)^2} P_{qq}\left(\frac{E_2}{E_2-E_3}\right) F_\text{LM}(1,2-3), \end{aligned} \tag{61}$$

where the splitting function P_{qq} is given by

$$P_{qq}(z) = C_F\left(\frac{1+z^2}{1-z} - \epsilon(1-z)\right). \tag{62}$$

Note that the $\mathcal{O}(\epsilon)$ term that appears in P_{qq} in Eq. (62) is the consequence of additional gluon polarizations that need to be accounted for in case of the $(4-2\epsilon)$-dimensional space-time.

We now use the operators introduced in Eq. (61) to subtract soft and collinear singularities. It is convenient to denote integration over the relevant phase spaces, continued to d dimensions, using angle brackets

$$\mathrm{d}\sigma_R = \langle F_{\rm LM}(1,2,3)\rangle. \tag{63}$$

As we already discussed, $\mathrm{d}\sigma_R$ can not be computed in four-dimensional space-time since it exhibits soft and collinear singularities. To isolate them, we rewrite Eq. (63) in the following way

$$\begin{aligned}\langle F_{\rm LM}(1,2,3)\rangle &= \langle (I-S_3)F_{\rm LM}(1,2,3)\rangle + \langle S_3 F_{\rm LM}(1,2,3)\rangle \\ &= \langle (I-C_{31}-C_{32})(I-S_3)F_{\rm LM}(1,2,3)\rangle \\ &+ \langle (C_{31}+C_{32})(I-S_3)F_{\rm LM}(1,2,3)\rangle + \langle S_3 F_{\rm LM}(1,2,3)\rangle,\end{aligned} \tag{64}$$

where I is an identity operator. It is instructive to explore different terms on the right hand side of Eq. (64) keeping an eye on the simplifications in hard matrix elements that occur once soft and collinear operators act on $F_{\rm LM}(1,2,3)$.

First, we note that the term

$$\langle \mathcal{O}_{\rm NLO} F_{\rm LM}(1,2,3)\rangle = \langle (I-C_{31}-C_{32})(I-S_3)F_{\rm LM}(1,2,3)\rangle \tag{65}$$

does not have infra-red and collinear singularities and, therefore, can be computed in four dimensions. This is so because all the potentially singular limits are subtracted from the hard matrix element. Note that it is important to perform the subtraction in a "nested" way, i.e. the collinear subtraction is applied to the *soft-subtracted* matrix element squared.

The remaining two terms in Eq. (64) depend on the *simplified* matrix elements where gluon momentum does not appear at all (soft subtraction) or changes the energy of the incoming partons (collinear subtraction). Therefore, one can integrate these terms over some parts of the gluon phase-space without specifying the hard matrix element. Before we discuss this step in detail, we would like to simplify Eq. (64). To this end, we rewrite the last two terms in the following way

$$\begin{aligned}&\langle (C_{31}+C_{32})(I-S_3)F_{\rm LM}(1,2,3)\rangle + \langle S_3 F_{\rm LM}(1,2,3)\rangle \\ &= \langle (C_{31}+C_{32})F_{\rm LM}(1,2,3)\rangle + \langle (I-C_{31}-C_{32})S_3 F_{\rm LM}(1,2,3)\rangle,\end{aligned} \tag{66}$$

and focus on the last term. Taking $S_3 F_{\rm LM}(1,2,3)$ from Eq. (61), we compute

$$\begin{aligned}C_{31}S_3 F_{\rm LM}(1,2,3) &= g_s^2 C_F \frac{2E_1}{E_3(p_1p_3)} F_{\rm LM}(1,2), \\ C_{32}S_3 F_{\rm LM}(1,2,3) &= g_s^2 C_F \frac{2E_2}{E_3(p_2p_3)} F_{\rm LM}(1,2),\end{aligned} \tag{67}$$

For the head-on collisions, we find

$$\frac{2E_1}{E_3(p_1p_3)} + \frac{2E_2}{E_3(p_2p_3)} = \frac{2E_1(p_2p_3)+2E_2(p_1p_3)}{E_3(p_1p_3)(p_2p_3)} = \frac{2p_1p_2}{(p_3p_1)(p_2p_1)}. \tag{68}$$

Therefore,

$$\langle (I-C_{31}-C_{32})S_3 F_{\rm LM}(1,2,3)\rangle = 0, \tag{69}$$

which implies a simplified subtraction formula

$$\langle F_{\rm LM}(1,2,3)\rangle = \langle \mathcal{O}_{\rm NLO} F_{\rm LM}(1,2,3)\rangle + \langle (C_{31}+C_{32})F_{\rm LM}(1,2,3)\rangle. \tag{70}$$

As we already mentioned, the first term on the right hand side of Eq. (70) is finite and can be computed in a straightforward way. We will now study the collinear subtraction terms.

We take $\langle C_{31}F_{\rm LM}(1,2,3)\rangle$ as an example and write

$$\begin{aligned}\langle C_{31}F_{\rm LM}(1,2,3)\rangle &= \int [{\rm d}p_3]\frac{g_s^2}{(p_1-p_3)^2}P_{qq}\left(\frac{E_1}{E_1-E_3}\right)(2s)^{-1}F_{\rm LM}(1-3,2)\\ &= \int \frac{E_3^{d-3}{\rm d}E_3\,{\rm d}\Omega^{(d-1)}}{2(2\pi)^{d-1}}\frac{g_s^2}{-2E_1E_3(1-\cos\theta_{13})}P_{qq}\left(\frac{E_1}{E_1-E_3}\right)(2s)^{-1}F_{\rm LM}\left(\frac{E_1-E_3}{E_3}1,2\right).\end{aligned} \tag{71}$$

Since $F_{\rm LM}(1-3,2)$ is independent of the gluon emission angle, we can integrate over it. This is a typical simplification that occurs with the subtraction terms since hard matrix elements in the subtraction terms depend on a limited number of gluon kinematic variables, if at all. Integration over the gluon emission angle is straightforward and we obtain

$$\int \frac{{\rm d}\Omega^{(d-1)}}{1-\cos\theta_{13}} = -\Omega^{(d-2)}\frac{2^{-2\epsilon}\Gamma^2(1-\epsilon)}{\epsilon\,\Gamma(1-2\epsilon)}. \tag{72}$$

The $1/\epsilon$ factor that appears after the integration over angle is the collinear divergence that we discussed earlier.

The remaining integration over energy of the emitted gluon in Eq. (71) can not be performed without specifying the hard matrix element. However, it is possible to write the integrand in Eq. (71) in a more transparent way by changing the integration variable. We write $E_3 = E_1(1-z)$ and use $P_{qq}(1/z) = -P_{qq}(z)/z$ which can be verified using explicit expression for the splitting function in Eq. (62). Putting everything together, we obtain

$$\langle C_{31}F_{\rm LM}(1,2,3)\rangle = -\frac{[\alpha_s]}{\epsilon}\frac{\Gamma^2(1-\epsilon)}{\Gamma(1-2\epsilon)}(2E_1)^{-2\epsilon}\int\limits_{z_{\rm min}}^1 \frac{{\rm d}z}{(1-z)^{2\epsilon}}P_{qq}(z)\,\langle\frac{F_{\rm LM}(z\cdot 1,2)}{z}\rangle, \tag{73}$$

where

$$[\alpha_s] = \frac{\alpha_s\mu^{2\epsilon}e^{\epsilon\gamma_E}}{2\pi\Gamma(1-\epsilon)}, \tag{74}$$

is the strong coupling constant at the scale μ and $z_{\rm min} = 1 - E_{\rm max}/E_1$.

A glance at the splitting function in Eq. (62) reveals that the remaining integration in Eq. (73) leads to divergences. Indeed, in the $z\to 1$ limit, $P_{qq}\sim 2C_F/(1-z)$, so that the integration over z can not be preformed in four dimensions. The first thing we need to do is to extract the $z\to 1$ singularity without specifying the hard matrix element. This is easy to accomplish – since this singularity is logarithmic it can be easily subtracted. More precisely, we split the P_{qq} function into singular and regular parts and write

$$P_{qq} = \frac{2C_F}{1-z} + P_{qq}^{\rm reg}, \quad P_{qq}^{\rm reg} = -C_F(1+z+\epsilon(1-z)). \tag{75}$$

Then, we introduce a new notation $G(z) = \langle F_{\rm LM}(z\cdot 1,2)/z\rangle$ and write the relevant integral as

$$\int\limits_{z_{\rm min}}^1 \frac{{\rm d}z}{(1-z)^{2\epsilon}}P_{qq}(z)\,G(z) = \int\limits_0^1 {\rm d}z\left[\frac{2C_F}{(1-z)^{1+2\epsilon}} + (1-z)^{-2\epsilon}P_{qq}^{\rm reg}\right]G(z). \tag{76}$$

Note that we replaced $z_{\rm min}$ with zero, as the lower integration boundary; this is allowed because the minimal value of z is determined by the energy-momentum conservation condition for the process $q(zp_1)+\bar{q}(p_2)\to l^+l^-$ which implies that a non-vanishing energy of the incoming quark is required to produce a pair of leptons.

The first term on the right hand side in Eq. (76) requires further analysis; the second term does not lead to singularities and, therefore, can be integrated numerically, expanding around $d = 4$. To deal with the first term, we write

$$\begin{aligned}\int_0^1 \mathrm{d}z\ \frac{2C_F}{(1-z)^{1+2\epsilon}} G(z) &= \int_0^1 \mathrm{d}z\ \frac{2C_F}{(1-z)^{1+2\epsilon}} \left(G(z) - G(1)\right) - \frac{C_F}{\epsilon} G(1) \\ &= -\frac{C_F}{\epsilon}\, G(1) + 2C_F \sum_{n=0}^{\infty} \frac{(-1)^n (2\epsilon)^n}{n!} \int_0^1 \mathcal{D}_n(z) G(z).\end{aligned} \tag{77}$$

In the last step we introduced the so-called "plus"-distributions that are defined as follows

$$\mathcal{D}_n(z) = \left[\frac{\ln^n(1-z)}{1-z}\right]_+ \Rightarrow \qquad \int_0^1 \mathrm{d}z\ \mathcal{D}_n(z)\ G(z) = \int_0^1 \mathrm{d}z\ \frac{\ln^n(1-z)}{(1-z)} \left[G(z) - G(1)\right]. \tag{78}$$

Clearly, these distributions provide a way to regulate an integral that otherwise diverges at $z = 1$.

Putting everything together and expanding the result in powers of ϵ up to $\mathcal{O}(\epsilon^0)$, we obtain the following expression for the collinear subtraction term

$$\begin{aligned}\langle C_{31} F_{\rm LM}(1,2,3)\rangle = -\frac{[\alpha_s]}{\epsilon} \frac{\Gamma^2(1-\epsilon)}{\Gamma(1-2\epsilon)}\ s^{-\epsilon} \Bigg[\left(-\frac{C_F}{\epsilon} + \frac{3C_F}{2}\right) \langle F_{\rm LM}(1,2)\rangle \\ + \int_0^1 \mathrm{d}z P_{qq,R}(z) \langle \frac{F_{\rm LM}(z\cdot 1, 2)}{z}\rangle \Bigg],\end{aligned} \tag{79}$$

where

$$P_{qq,R}(z) = P_{qq}^{(0)} + \epsilon P_{qq,R}^{\epsilon}(z) + \mathcal{O}(\epsilon^2), \tag{80}$$

and

$$\begin{aligned}P_{qq}^{(0)} &= C_F \left(2D_0(z) - (1+z) + \frac{3}{2}\delta(1-z)\right), \\ P_{qq,R}^{(\epsilon)}(z) &= C_F \left(2(1+z)\log(1-z) - (1-z) - 4D_1(z)\right).\end{aligned} \tag{81}$$

A similar analysis can be performed for the emission off the incoming anti-quark. Combining the relevant formulas, we derive the result for the real emission cross section

$$\begin{aligned}2s\mathrm{d}\sigma^R =& 2[\alpha_s] s^{-\epsilon} \left(\frac{C_F}{\epsilon^2} + \frac{3C_F}{2\epsilon}\right) \times \frac{\Gamma^2(1-2\epsilon)}{\Gamma(1-2\epsilon)} \langle F_{\rm LM}(1,2)\rangle \\ &- \frac{[\alpha_s] s^{-\epsilon}}{\epsilon} \frac{\Gamma(1-\epsilon)^2}{\Gamma(1-2\epsilon)} \int_0^1 \mathrm{d}z\ P_{qq}^{(0)}(z) \langle \frac{F_{\rm LM}(z1,2)}{z} + \frac{F_{\rm LM}(1,z2)}{z}\rangle \\ &- [\alpha_s] s^{-\epsilon} \frac{\Gamma(1-\epsilon)^2}{\Gamma(1-2\epsilon)} \int_0^1 \mathrm{d}z\ P_{qq,R}^{(\epsilon)}(z) \langle \frac{F_{\rm LM}(z1,2)}{z} + \frac{F_{\rm LM}(1,z2)}{z}\rangle \\ &+ \langle \mathcal{O}_{\rm NLO} F_{\rm LM}(1,2,4)\rangle.\end{aligned} \tag{82}$$

Terms on the right hand side in Eq. (82) are written as an expansion in $1/\epsilon$. We note that the strongest singularity $\mathcal{O}(1/\epsilon^2)$ appears in terms that depend on the cross section of the elastic (no-emission) process

$q\bar{q} \to e^+e^-$ in leading order kinematics. We also note that there is a large number of terms in Eq. (82) that exhibit $\mathcal{O}(1/\epsilon)$ singularities and depend on cross sections of the leading order process in the *boosted* kinematics, i.e. when a quark with reduced energy annihilates with an anti-quark, or vice versa.

As it is clearly seen from Eq. (82), the partonic process with additional gluon radiated into a final state leads to divergent contribution to the production cross section. If perturbative approach to hard hadron collisions is to make sense, there should be other contributions that cancel the singularities. What are these additional contributions? Clearly, for the cancellation of the divergent terms to happen, the relevant pieces must at the very least have a similar dependence on the hard scattering cross section as divergent terms in Eq. (82). Since the most singular term has tree-level kinematics, it is reasonable to imagine that *virtual corrections* to leading order process may produce a divergent result and, hopefully, cancel the singularities in the integrated real-emission cross section.

We can compute the virtual corrections to $q\bar{q} \to e^+e^-$ process explicitly and it may be, in fact, necessary to do so if we want to understand their contribution to dilepton pair production fully. However, if we are interested in understanding how divergences in real and virtual contributions cancel out, there is a better way. Indeed, it was pointed out by S. Catani [17] that infra-red divergences of one-loop amplitudes in QCD are known for a generic process. Such infra-red divergences depend on the color charges of external particles, certain kinematic invariants and leading order scattering amplitudes. In case of dilepton pair production, the scattering amplitude can be written as

$$\mathcal{M}_{\rm full} = \mathcal{M}_0 + \frac{\alpha_s(\mu)}{2\pi}\mathcal{M}_{1-\rm loop} + \mathcal{O}(\alpha_s^2), \qquad \mathcal{M}_{1-\rm loop} = I_1(\epsilon)\mathcal{M}_0 + \mathcal{M}^{\rm fin}_{1-\rm loop}, \tag{83}$$

where

$$I_1(\epsilon) = -\frac{e^{\epsilon\gamma_E}}{\Gamma(1-\epsilon)}\left[\frac{C_F}{\epsilon^2} + \frac{3C_F}{2\epsilon}\right]\left(\frac{\mu^2}{-s-i0}\right)^{-\epsilon}. \tag{84}$$

Squaring the amplitude and accounting for the interference between $\mathcal{M}_0$ and $\mathcal{M}_{1-\rm loop}$, we obtain the following result for the virtual corrections to leading order cross section

$$2s{\rm d}\sigma_V = -2[\alpha_s]\cos(\epsilon\pi)\left(\frac{C_F}{\epsilon^2} + \frac{3C_F}{2\epsilon}\right)s^{-\epsilon}\langle F_{\rm LM}(1,2)\rangle + \langle F^{\rm fin}_{LV}(1,2)\rangle. \tag{85}$$

The last term on the right hand side represents the finite contribution that can be computed in four dimensions; all $1/\epsilon$ divergences that appear in virtual contributions to cross sections are shown explicitly.

To compute the rate, we combine real Eq. (82) and virtual Eq. (85) corrections. It is easy to see that divergent parts of virtual corrections and contributions to real emission corrections proportional to $\langle F_{\rm LM}(1,2)\rangle$ cancel almost entirely. Expanding in ϵ, we find

$$\begin{aligned}
2s{\rm d}\sigma^{R+V} &= -\frac{[\alpha_s]s^{-\epsilon}}{\epsilon}\frac{\Gamma(1-\epsilon)^2}{\Gamma(1-2\epsilon)}\int\limits_0^1 {\rm d}z\; P^{(0)}_{qq}(z)\langle\frac{F_{\rm LM}(z1,2)}{z} + \frac{F_{\rm LM}(1,z2)}{z}\rangle \\
&+ \frac{2\pi^2 C_F}{3}\frac{\alpha_s}{2\pi}\langle F_{\rm LM}(1,2)\rangle - \frac{\alpha_s}{2\pi}\int\limits_0^1 {\rm d}z\; P^{(\epsilon)}_{qq,R}(z)\langle\frac{F_{\rm LM}(z1,2)}{z} + \frac{F_{\rm LM}(1,z2)}{z}\rangle \\
&+ \langle\mathcal{O}_{\rm NLO}F_{\rm LM}(1,2,3)\rangle.
\end{aligned} \tag{86}$$

As can be seen from Eq. (86), the remaining divergences are associated with tree-level cross sections for dilepton pair production that, however, describe a situation where a pair is boosted along the collision axis. A boost along the collision axis changes rapidity distribution and can, in principle, be absorbed into a re-definition of parton distribution functions. Indeed, we have seen in discussing the leading order cross section that parton distribution functions determine the rapidity distribution of dilepton pairs.

When we talked about the leading order cross section, we said that parton distribution functions are universal non-perturbative objects that are determined in experiment. What does it mean then, that they can be changed to absorb divergent contributions to partonic cross sections? Well, the point is that theoretical predictions for experimental quantities *include* divergent contributions – what is measured in the experiment is a combination of *bare* parton distribution functions and the divergent terms that appear in perturbative computations. It is the combination of the two that defines physical parton distribution functions.

Therefore, similar to all other parameters that appear in perturbative computations in Quantum Field Theory, we start with the so-called bare parton distribution functions and write them as physical parton distributions and the counter-terms whose role is to remove the divergences. Similar to ordinary ultraviolet renormalization in Quantum Field Theory, counter-terms for parton distribution functions lead to the renormalization group equation which in this case is known as Dokshitzer-Gribov-Altarelli-Parisi (DGLAP) evolution equation [18]. We will talk about this equation in Section 6. For now, we just quote the relation between bare and renormalized parton distribution functions that we use to remove remaining singularities in the NLO cross section Eq.(86). The renomalization of parton distribution functions amounts to the replacement

$$f_i^{\rm bare} \to \left[\hat{\delta}_{ij} + \frac{\alpha_s(\mu)}{2\pi\epsilon} P_{ij}^{(0)} + \mathcal{O}(\alpha_s^2)\right] \otimes f_j(\mu), \tag{87}$$

where summation over repeated index is assumed and the convolution is defined as follows

$$\left[f_1 \otimes f_2\right](z) = \int_0^1 {\rm d}x_1 {\rm d}x_2 f_1(x_1) f_2(x_2) \delta(z - x_1 x_2). \tag{88}$$

Since we consider $q\bar{q}$ collisions, the function $P_{ij}^{(0)}$ needs to be substituted with the Altarelli-Parisi kernels $P_{qq}^{(0)}$ Eq. (81). In fact, a glance at Eq. (86) shows that the remaining divergences in our computation are proportional to $P_{qq}^{(0)}$ and have exactly the right form to be canceled by the renormalization of parton distribution functions Eq. (87). We use Eq. (87) in leading order cross section, expand it through $\mathcal{O}(\alpha_s)$ and combine the additional terms with the NLO cross section Eq. (86). We observe that all $1/\epsilon$ terms cancel and we find

$$\begin{aligned} 2s{\rm d}\sigma^{\rm NLO} &= \langle F_{\rm LV}^{\rm fin}(1,2) + \frac{\alpha_s}{2\pi}\frac{2\pi^2}{3} C_F F_{\rm LM}(1,2)\rangle + \langle \mathcal{O}_{\rm NLO} F_{\rm LM}(1,2,4)\rangle \\ &+ \frac{\alpha_s}{2\pi}\int_0^1 {\rm d}z \left[P_{qq}^{(0)}(z)\ln\frac{s}{\mu^2} - P_{qq,R}^{(\epsilon)}(z)\right] \langle \frac{F_{\rm LM}(z1,2)}{z} + \frac{F_{\rm LM}(1,z2)}{z}\rangle. \end{aligned} \tag{89}$$

Since the NLO contribution to the partonic cross section Eq.(89) contains no $1/\epsilon$ singularities, all quantities there can be computed in four-dimensional space-time. We note that Eq. (89) provides a fully-differential cross-section for the lepton pair production in partonic collisions since no integration over resolved phase-space has been performed there. The NLO contribution to the hadronic cross section is obtained by convoluting the differential partonic cross section Eq. (89) with parton distribution functions.

Computation of NLO QCD corrections to dilepton pair production described in this Section shows the importance of soft and collinear limits of the matrix elements for computing physical infra-red safe quantities. Although our discussion focused on a particular process, it's main ingredients are universal and can be used to construct a *general algorithm* for NLO computations [10, 11]. Extensions of these approaches to even higher orders are also possible; in fact, recently several methods were proposed that can be used to perform fully-differential NNLO QCD computations [14]. Making these methods computationally more efficient is very important for extending their applicability to more complex processes and significant effort currently goes into that.

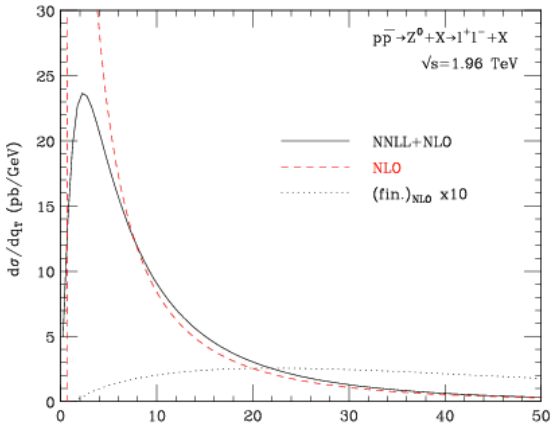

Fig. 6: Transverse momentum distribution of a lepton pair at the Tevatron. Fixed order and resummed results are compared [20].

Going back to our result Eq. (89), we can ask what will happen if we use it to compute kinematic distributions of a lepton pair. Recall that we started thinking about NLO QCD contribution to dilepton production cross section because the leading order result did not properly describe the transverse momentum distribution of a lepton pair. Using next-to-leading order predictions for the cross section, we find a refined description of the invariant mass and the rapidity distributions of a lepton pair. Although its qualitative features are similar to what we observed at leading order, they describe experimental data much better and their dependence on unphysical parameters such as the renormalization and the factorizations scales is significantly reduced. We also find a non-trivial transverse momentum distribution as shown in Fig. 6 which is a clear improvement over the leading order result. However, although the NLO QCD distribution provides a decent description of the experimental results (cf. Fig. 5) at high $p_\perp$, it keeps growing with the decrease of the transverse momentum in contrast to the experimental result that reaches maximum at finite $p_\perp$ and decrease after that. Therefore, in comparison to leading order computations, we have a partial success with understanding the $p_\perp$-spectrum of dilepton pairs since, apparently, its high-$p_\perp$ region is amenable to perturbative treatment, whereas something more complex occurs at low transverse momenta. We will try to understand what is happening there in the next Section.

5 Small-$p_\perp$ resummation

We will discuss the small-$p_\perp$ region in the context of QED, ignoring all complications related to the non-Abelian nature of QCD. However, the result that we will get will be valid in QCD as well provided that we trade electric charges for color ones. The QED analysis that we describe below follows the classic paper by Parisi and Petronzio [21]; their discussion of the problem was instrumental in setting up the stage for a modern understanding of small-$p_\perp$ resummation that is a very important topic for applications of perturbative QCD to hadron collider processes (see e.g. Ref. [22] for contemporary perspective).

We consider production of muon pairs in electron-positron collisions. We assume that muons are heavy and do not radiate photons. We are interested in understanding QED effects that are related to initial state radiation. This is very similar to gluon emissions in $q\bar{q}$ annihilation to lepton pairs studied in the previous Section.

We are interested in the transverse momentum distribution of a muon pair in the limit when the transverse momentum of a pair $p_\perp$ becomes very small. We will see that in each order of perturbation theory there are terms that contain *two* powers of $L = \log s/p_\perp^2 \gg 1$ per power of $\alpha \ll 1$. As the transverse momentum decreases, the logarithm increases whereas α stays fixed. Hence, we can reach

values of $p_\perp$ such that

$$\alpha L^2 \sim 1, \quad \alpha L \ll 1. \tag{90}$$

The appearance of αL^2 in each order of perturbative expansion does not allow us to truncate the series and forces us to resum contributions to perturbative cross sections that scale as $\sigma^{(k)} \sim \sigma_0 \ \alpha^k L^{2k} \sim \sigma_0, \quad k = 0, 1, 2, ...$ Clearly, all other contributions, for examples $\sigma^{(k)} \sim \sigma_0 \ \alpha^{k+1} L^{2k} \sim \alpha \ \sigma_0 \ll \sigma_0$, are small and can be neglected.

Two powers of $p_\perp$-dependent logarithms per power of α can only be generated by photon emissions that are *soft and collinear at the same time*. As we already know from the previous Section, a single *soft* photon emission can be described by the eikonal factor

$$\lim_{k\to 0} \overline{|\mathcal{M}(e^+, e^-; k)|}^2 \approx e^2 \frac{2p_1p_2}{(p_1k)(p_2k)} \overline{|\mathcal{M}(e^+, e^-)|}^2. \tag{91}$$

Consider now the head-on collision where $p_1 = (E_1, 0, 0, E_1)$ and $p_2 = (E_2, 0, 0, -E_2)$. We parametrize the photon momentum as $k = \omega(1, \sin\theta\cos\phi, \sin\theta\sin\phi, \cos\theta)$. The eikonal factor becomes

$$\frac{2p_1p_2}{(p_1k)(p_2k)} = \frac{4E_1E_2}{E_1E_2\omega^2(1-\cos\theta)(1+\cos\theta)} = \frac{4}{\vec{k}_\perp^2}, \tag{92}$$

where we used $|\vec{k}_\perp| = \omega \sin\theta$ for the absolute value of the photon transverse momentum. Hence, we find

$$|\mathcal{M}(e^+, e^-; k)|^2 \approx \frac{4e^2}{\vec{k}_\perp^2} \ |\mathcal{M}(e^+, e^-)|^2. \tag{93}$$

We need to understand what happens if we integrate the radiation amplitude squared Eq. (93) over the photon phase space. Since the photon is soft we can neglect the photon momentum k in the δ-function that enforces energy-momentum conservation. We then identify the $\mu^+\mu^-$ transverse momentum $p_\perp$ with the photon transverse momentum. The phase space element reads

$$\frac{\mathrm{d}^3k}{(2\pi)^3 2\omega} = \frac{\mathrm{d}\cos\theta \mathrm{d}\phi \omega \mathrm{d}\omega}{16\pi^3} = \frac{1}{8\pi^2} \ \mathrm{d}\cos\theta \ \omega \mathrm{d}\omega. \tag{94}$$

Since $k_\perp = \omega \sin\theta$, we can express the emission angle θ in terms of the transverse momentum

$$\cos\theta = \pm\sqrt{1 - \frac{k_\perp^2}{\omega^2}}. \tag{95}$$

Changing variables $\cos\theta \to k_\perp$ in Eq. (94), we obtain

$$\frac{\mathrm{d}^3k}{(2\pi)^3 2\omega} = \frac{1}{8\pi^2} \frac{2k_\perp \mathrm{d}k_\perp \mathrm{d}\omega}{\sqrt{\omega^2 - k_\perp^2}}. \tag{96}$$

We are interested in computing the real-emission cross section in the logarithmic approximation. Therefore, we write

$$\frac{\mathrm{d}\omega}{\sqrt{\omega^2 - k_\perp^2}} \approx \frac{\mathrm{d}\omega}{\omega}. \tag{97}$$

Integration over ω will have to be cut at $\omega \approx k_\perp$ from below and at $\omega \approx \sqrt{s}$ from above. The first condition follows from the approximation in Eq. (97); the second condition from the requirement that the emitted photon is soft.

Combining the matrix element with the phase space parametrization we obtain

$$\frac{\mathrm{d}\sigma_\gamma}{\mathrm{d}k_\perp^2} = \sigma_0 \frac{2\alpha}{\pi}\frac{1}{k_\perp^2}\int\limits_{k_\perp}^{\sqrt{s}} \frac{\mathrm{d}\omega}{\omega} = \sigma_0 \frac{\alpha}{\pi}\frac{\ln\frac{s}{k_\perp^2}}{k_\perp^2}. \tag{98}$$

This formula shows once again that the transverse momentum distribution computed through first order in perturbation theory grows strongly in the limit $k_\perp \to 0$. In fact, the growth is so strong that is can overcome suppression provided by the fine structure constant α and make the radiation cross section larger than the Born one. Clearly, perturbative expansion in α becomes meaningless in this case.

It is important to understand the role of virtual corrections in shaping the transverse momentum distribution. The virtual corrections reside at $k_\perp = 0$. To understand how they can be included in our computation, we calculate the cross section to produce a $\mu^+\mu^-$ pair with a transverse momentum between 0 and $p_\perp$. We define

$$\Sigma(p_\perp) = \frac{1}{\sigma_0}\int\limits_0^{p_\perp^2} \frac{\mathrm{d}\sigma_{\mathrm{tot}}}{\mathrm{d}k_\perp^2}\mathrm{d}k_\perp^2. \tag{99}$$

Expanding the total cross section in powers of α and introducing $\mathrm{d}\sigma_{\gamma+V}$ to denote $\mathcal{O}(\alpha)$ contribution to the cross section that includes both real emission and virtual corrections, we write

$$\Sigma(p_\perp) - 1 = \frac{1}{\sigma_0}\int\limits_0^{p_\perp^2} \frac{\mathrm{d}\sigma_{\gamma+V}}{\mathrm{d}k_\perp^2}\mathrm{d}k_\perp^2 = \frac{1}{\sigma_0}\int\limits_0^{s} \frac{\mathrm{d}\sigma_{\gamma+V}}{\mathrm{d}k_\perp^2}\mathrm{d}k_\perp^2 - \frac{1}{\sigma_0}\int\limits_{p_\perp^2}^{s} \frac{\mathrm{d}\sigma_{\gamma}}{\mathrm{d}k_\perp^2}\mathrm{d}k_\perp^2 \tag{100}$$

The first term – given by an integral from 0 to s represents the radiative correction to the total cross section for $\mu^+\mu^-$ production in the logarithmic approximation, with both real and virtual corrections included. Such corrections contain no large logarithms and, since we only care about terms that scale as αL^2, can be set to zero. This identification, effectively, provides an infra-red regularization prescription that allows us to define the integrand at $k_\perp^2 = 0$ *without computing virtual corrections*. Thus, we require

$$\frac{1}{\sigma_0}\int\limits_0^{s} \frac{\mathrm{d}\sigma_{\gamma+V}}{\mathrm{d}k_\perp^2}\mathrm{d}k_\perp^2 = \mathcal{O}(\alpha_s) \Rightarrow 0, \tag{101}$$

and use Eq. (100) to derive

$$\Sigma(p_\perp) = 1 - \frac{\alpha}{2\pi}\ln^2\frac{s}{p_\perp^2}. \tag{102}$$

It is possible to re-write the integrand in Eq. (100) in such a way that Eq. (102) is obtained by the direct integration. The idea is to introduce the plus-distribution. We define

$$\frac{\mathrm{d}\sigma}{\sigma_0 \mathrm{d}k_\perp^2} = \delta(k_\perp^2) + \frac{\alpha}{\pi}\left[\frac{1}{k_\perp^2}\ln\frac{s}{k_\perp^2}\right]_+, \tag{103}$$

where the $+$-prescription is defined on an interval $k_\perp^2 \in [0, s]$. To illustrate how this works, we compute the total cross section using Eq. (103). We find

$$\begin{aligned}\Sigma(s^{1/2}) &= \frac{1}{\sigma_0}\int\limits_0^{s} \frac{\mathrm{d}\sigma}{\mathrm{d}k_\perp^2}\mathrm{d}k_\perp^2 = \int\limits_0^{s}\mathrm{d}k_\perp^2\left(\delta(k_\perp^2) + \frac{\alpha}{\pi}\left[\frac{1}{k_\perp^2}\ln\frac{s}{k_\perp^2}\right]_+\right)\\ &= 1 + \frac{\alpha}{\pi}\int\limits_0^{s}\frac{\mathrm{d}k_\perp^2}{k_\perp^2}\ln\left(\frac{s}{k_\perp^2}\right)(1-1) = 1.\end{aligned} \tag{104}$$

To extend this result to higher orders in α, we need to understand multiple photon emissions in the soft approximation. It is well-known [5] that soft photon emissions completely factorize so that a n-photon emission amplitude reads

$$\mathcal{M}_n = e^n \prod_{i=1}^{n} \left(\frac{p_1\epsilon_i}{p_1 k_i} - \frac{p_2\epsilon_i}{p_2 k_i} \right) \mathcal{M}_0. \tag{105}$$

Here ϵ_i and k_i are the polarization vector and the four-momentum of the i-th photon, respectively. Squaring $\mathcal{M}_n$ and summing over photon polarizations, we obtain

$$\sum_{\text{pol}} |\mathcal{M}_n|^2 = |\mathcal{M}_0|^2 \prod_{i=1}^{n} e^2 \frac{2p_1p_2}{(p_1k_i)(p_2k_i)} \tag{106}$$

It follows from Eq. (106) that the emission probability of each of the n photons is determined by an eikonal factor studied at the beginning of this Section. We use the expression for the amplitude squared to compute the transverse momentum distribution of the muon pair. It reads

$$\frac{1}{\sigma_0}\frac{\mathrm{d}^2\sigma_n}{\mathrm{d}^2\vec{p}_\perp} = \frac{1}{n!}\int \prod_{i=1}^{n} \frac{\mathrm{d}^3\vec{k}_i}{(2\pi)^3 2\omega_i} \left[\frac{e^2 2p_1p_2}{(p_1\cdot k_i)(p_2\cdot k_i)} \right] \delta^{(2)}\left(\vec{p}_\perp - \sum_i^n \vec{k}_{\perp,i} \right). \tag{107}$$

To proceed further, we need to find a way to factorize the δ-function that contains the sum of photon transverse momenta preventing us from integrating over any of them. To this end, we write the δ-function as an integral over auxiliary two-component vector that we will refer to as the "impact parameter"

$$\delta^{(2)}\left(\vec{p}_\perp - \sum \vec{k}_{i,\perp} \right) = \int \frac{\mathrm{d}^2\vec{b}}{(2\pi)^2} e^{-i\vec{b}\left(\vec{p}_\perp - \sum\limits_{i=1}^{n} \vec{k}_{i,\perp} \right)}. \tag{108}$$

Using this equation, we re-write the cross section for emitting n-photon, integrating along the way over their energies. We find

$$\frac{1}{\sigma_0}\frac{\mathrm{d}^2\sigma_n}{\mathrm{d}^2\vec{p}_\perp} = \frac{1}{n!}\int \frac{\mathrm{d}^2\vec{b}}{(2\pi)^2} e^{-i\vec{b}\vec{p}_\perp} \left[\frac{\alpha}{\pi} \int \frac{\mathrm{d}^2\vec{k}_\perp}{\pi\vec{k}_\perp^2} \ln\frac{s}{k_\perp^2}\, e^{-i\vec{b}\vec{k}_\perp} \right]^n, \tag{109}$$

where the integration over $k_\perp$ is cut at $k_\perp^2 = s$. The apparent singularity at $k_\perp = 0$ is regulated in the same way as in case of the single photon emission – we introduce a plus-prescription ensuring the cancellation of real and virtual corrections for fully inclusive quantities.

It is clear from Eq. (109) that the summation over n can be performed in a straightforward manner. We obtain

$$\frac{\mathrm{d}\sigma}{\sigma_0 \mathrm{d}^2\vec{p}_\perp} = \sum_{n=0}^{\infty} \frac{\mathrm{d}^2\sigma_n}{\sigma_0 \mathrm{d}^2\vec{p}_\perp} = \int \frac{\mathrm{d}^2\vec{b}}{(2\pi)^2} e^{-i\vec{b}\vec{p}_\perp} \hat{\sigma}(b), \tag{110}$$

where

$$\hat{\sigma}(b) = e^{\frac{\alpha}{\pi}\nu(b)}, \qquad \nu(b) = \int_0^{|k_\perp|<\sqrt{s}} \frac{\mathrm{d}^2\vec{k}_\perp}{\pi} \left[\frac{1}{k_\perp^2} \ln\frac{s}{k_\perp^2} \right]_+ e^{i\vec{b}\vec{k}_\perp}. \tag{111}$$

The result given in Eq. (110) is the differential cross section for producing a muon pair with momentum $p_\perp$ in the double logarithmic approximation. This formula is implicit because of the integration over the impact parameter. In what follows, we will compute some of the integrals explicitly and arrive at the result for the cross section that is more transparent. In particular, we are interested in understanding if the differential cross section in Eq. (110) exhibits a turnover at low values of the transverse momentum, a feature that was clearly missing in the result of the next-to-leading order computation.

To proceed with sufficiently complicated integrations in Eq. (110), we note that the integrals in Eqs. (110,111) depend on $\vec{p}_\perp, \vec{b}$ and s. From Eq. (110) it follows that $b \sim 1/p_\perp$. Since $\sqrt{s} \gg p_\perp$, $sb^2 \gg 1$. We need to compute the various quantities in Eqs.(110,111) taking advantage of these hierarchical relations between the various parameters that appear there.

We begin with the computation of $\nu(b)$. We perform the angular integration and find

$$\begin{aligned}\nu(b) = &\int\limits_0^{|k_\perp|<\sqrt{s}} \frac{\mathrm{d}^2\vec{k}_\perp}{\pi}\left[\frac{1}{k_\perp^2}\ln\frac{s}{k_\perp^2}\right]_+ e^{i\vec{b}\vec{k}_\perp} = \int\limits_0^{|k_\perp|<\sqrt{s}} \frac{\mathrm{d}k_\perp^2}{k_\perp^2}\ln\frac{s}{k_\perp^2}\int\limits_0^{2\pi}\frac{\mathrm{d}\varphi}{2\pi}\left[e^{ibk_\perp\cos\varphi}-1\right]\\ &= \int\limits_0^{s}\frac{\mathrm{d}k_\perp^2}{k_\perp^2}\ln\frac{s}{k_\perp^2}\left[J_0(b_\perp k_\perp)-1\right],\end{aligned} \tag{112}$$

where $J_0(x)$ is the Bessel function of the first kind.[4] To make the integral more tractable, we change variables $k_\perp \to \xi = b_\perp k_\perp$ and obtain

$$\nu(b) = 2\int\limits_0^{\sqrt{s}b}\frac{\mathrm{d}\xi}{\xi}\ln\left[\frac{sb^2}{\xi^2}\right]\left[J_0(\xi)-1\right]. \tag{113}$$

We now integrate by parts, use $J_0(0)=1, \quad \mathrm{d}J_0(\xi)/\mathrm{d}\xi = -J_1(\xi)$, and find

$$\nu(b) = \frac{1}{2}\ln^2(sb^2)\left(J_0(\sqrt{s}b)-1\right) + 2\int\limits_0^{\sqrt{s}b}\mathrm{d}\xi\left[\ln(sb^2)\ln\xi - \ln^2\xi\right]J_1(\xi). \tag{114}$$

Since $J_0(\sqrt{s}b) \sim (\sqrt{s}b)^{-1/2}$ and since the integral with $J_1(\xi)$ converges at infinity, we can neglect quite a number of terms in Eq. (114) if we focus on the double logarithmic contributions. We find

$$\nu(b) \approx -\frac{1}{2}\ln^2(sb^2) + \mathcal{O}(\ln(sb^2)). \tag{115}$$

The cross section becomes

$$\frac{1}{\sigma_0}\frac{\mathrm{d}^2\sigma}{\mathrm{d}^2\vec{p}_\perp} = \int\frac{\mathrm{d}^2\vec{b}}{(2\pi)^2}e^{-i\vec{b}\vec{p}_\perp}e^{-\frac{\alpha}{2\pi}\ln^2(sb^2)} = \frac{1}{2\pi}\int\limits_0^\infty \mathrm{d}b\; b\; J_0(bp_\perp)\; e^{-\frac{\alpha}{2\pi}\ln^2(sb^2)}, \tag{116}$$

where in the last step we integrated over directions of the vector $\vec{b}$. To proceed further, we change integration variables $b \to y$ where $b = y/p_\perp$ and expand the integrand assuming that $\alpha\ln^2 s/p_\perp \sim 1$ but $\alpha \ln s/p_\perp \ll 1$. We obtain

$$\frac{1}{\sigma_0}\frac{\mathrm{d}^2\sigma}{\mathrm{d}^2\vec{p}_\perp} = \frac{1}{2\pi p_\perp^2}e^{-\frac{\alpha}{2\pi}\ln^2\frac{s}{p_\perp^2}}\int\limits_0^\infty \mathrm{d}y\; y\; J_0(y)\left(1-\frac{2\alpha}{\pi}\ln\frac{s}{p_\perp^2}\ln y + ...\right), \tag{117}$$

where ellipses stand for $\mathcal{O}(\alpha^2)$ terms that can be neglected. Integration over y can be performed using the known results for definite integrals of the Bessel functions

$$\int\limits_0^\infty \mathrm{d}y y J_0(y) = 0, \qquad \int\limits_0^\infty \mathrm{d}y J_0(y)\ln y = -1. \tag{118}$$

[4] Vast amount of information about special functions in general and Bessel functions in particular can be found in a classic book by Abramowitz and Stegun [23].

Using these results in Eq. (117), we derive the resummed cross section

$$\frac{1}{\sigma_0}\frac{\mathrm{d}^2\sigma}{\mathrm{d}^2\vec{p}_\perp} = \frac{\alpha}{\pi^2 p_\perp^2}\ln\frac{s}{p_\perp^2}e^{-\frac{\alpha}{2\pi}\ln^2\frac{s}{p_\perp^2}}. \tag{119}$$

It follows from Eq. (119) that the resummed $p_\perp$ distribution has a turnover, in contrast to the $p_\perp$ distribution that is predicted by a single photon emission. The distribution peaks at

$$p_\perp^{\max} \approx \sqrt{s}e^{-\frac{\pi}{2\alpha}}. \tag{120}$$

Note that $p_\perp^{\max}$ has a *non-analytic* dependence on the fine structure constant α and, for this reason, it can not be obtained in any finite order of perturbation theory.[5]

The transverse momentum distribution of a lepton pair in QED reflects all the subtleties of a resummed computation, but can be performed analytically until the very end thanks to the simplicity of this case. It is useful to take a look at the QCD formula that describes resummed transverse momentum distribution of a lepton pair in hadron collisions under the assumption that a pair is produced through a decay of an intermediate on-shell Z-boson; the Z-boson itself is produced in the $q\bar{q}$ annihilation. The resummed cross section reads [24]

$$\begin{aligned}\frac{\mathrm{d}\sigma_Z}{\mathrm{d}p_\perp^2} \approx \sum_q \frac{\sigma_0^{q\bar{q}}}{2}\int\limits_0^\infty \mathrm{d}b\, b\, J_0(bp_\perp)e^{-S(b,M_Z)}\int\limits_0^1 \mathrm{d}x_1\mathrm{d}x_2\delta\left(x_1x_2-\frac{M_Z^2}{S}\right)\\ \times\left[q(x_1,b_0/b)\bar{q}(x_2,b_0/b)+q\leftrightarrow\bar{q}\right],\end{aligned} \tag{121}$$

where s is the hadronic center-of-mass energy squared, $\sigma_0^{q\bar{q}} = \pi\sqrt{2}G_F M_Z^2(V_q^2+A_q^2)/(3S)$, $b_0 = 2e^{-\gamma_E}$ and

$$S(b,Q) = \int\limits_{(b_0/b)^2}^{Q^2}\frac{\mathrm{d}q^2}{q^2}\left[\ln\frac{Q^2}{q^2}A(\alpha_s(q))+B(\alpha_s(q))\right], \tag{122}$$

where the two functions A and B can be computed in QCD perturbation theory

$$A(\alpha_s) = \sum_{n=1}^\infty\left(\frac{\alpha_s}{2\pi}\right)^n A_n, \quad B(\alpha_s) = \sum_{n=1}^\infty\left(\frac{\alpha_s}{2\pi}\right)^n B_n. \tag{123}$$

It is easy to see the similarities between the resummed cross sections in QCD and QED. However, an interesting feature of the QCD result is the appearance of the transverse momentum in parton distribution functions. Indeed, since $b \sim p_\perp$ and since the *factorization scale* for parton distribution functions in Eq. (121) is chosen to be $1/b$, it appears that one can only resum the $\ln\sqrt{s}/p_\perp$ contributions provided that the factorization scale is proportional to $p_\perp$. We already mentioned the dependence of parton distribution functions on the factorization scale when we talked about fixed order computations and the relation between bare and physical parton distribution functions. In the next Section we will discuss the origin of parton distribution functions and the physical meaning of the factorization scale.

6 Partons and their evolution

We have seen in the previous Section that the resummed formula for the transverse momentum distribution includes parton distribution functions evaluated at a particular scale $1/b \sim p_\perp$ which is correlated with the transverse momentum of the produced lepton pair. If we want to understand why it is so, we

[5] However, the vaue of $p_\perp$ for which the distribution reaches its maximum is *outside* the validity range of our computation since $\alpha/\pi\ln(\sqrt{s}/p_\perp^{\max}) \sim 1$.

need to understand the physics behind parton distribution functions. Similar to the discussion in the previous Section, it is much easier to discuss this problem in QED first and then explain how the QED results generalize to the QCD case.

Consider a process where an electron collides with a target that we will denote as X and produces a final state with a photon and another particle Y, $e + X \to \gamma + Y$. We will be interested in a situation where the final state photon is emitted in the forward direction, i.e. it follows the momentum of the incoming electron. To describe this kinematic situation, we employ the *collinear* approximation to the matrix element squared that we already used when discussing the NLO QCD corrections to the Drell-Yan process. We write

$$\sum_{\rm pol} |\mathcal{M}_{e(p)+X\to\gamma+Y}|^2 \approx \frac{-2e^2}{(p-q)^2}\frac{1+z^2}{z(1-z)}\sum_{\rm pol}|\mathcal{M}_{e(zp)+X\to Y}|^2, \tag{124}$$

where q is the four-momentum of the emitted photon that is parametrized as

$$q = (1-z)p + \beta\bar{p} + q_\perp. \tag{125}$$

Here $(1-z)$ is the fraction of the original electron energy carried away by the photon. The photon emission angle θ_γ is assumed to be small. The transverse momentum and the component of the four-momentum q along the complementary light-cone direction $\bar{p}$, β, scale as $q_\perp/\sqrt{s} \sim \theta_\gamma \ll 1$ and $\beta \sim \theta_\gamma^2 \ll 1$.

We use the approximate formula for the matrix element squared Eq. (124) to compute the cross section

$$\begin{aligned}
{\rm d}\sigma_{e+X\to\gamma+Y} &= \int [{\rm d}q][{\rm d}p_Y](2\pi)^4\delta^{(4)}(p+p_X-q-p_Y)\frac{1}{4(p_X\cdot p)}\frac{1}{2}\sum_{\rm pol}|\mathcal{M}_{e(p)+X\to\gamma+Y}|^2 \\
&\approx \int [{\rm d}q][{\rm d}p_Y](2\pi)^4\delta^{(4)}(zp+p_X-p_Y)\frac{-2e^2}{(p-q)^2}\frac{1+z^2}{1-z}\frac{1}{4(p_X\cdot zp)}\frac{1}{2}\sum_{\rm pol}|\mathcal{M}_{e(zp)+X\to Y}|^2 \\
&\approx \int [{\rm d}q]\frac{-2e^2}{(p-q)^2}\frac{1+z^2}{1-z}\ {\rm d}\sigma(e(zp)+X\to Y).
\end{aligned} \tag{126}$$

To arrive at the final formula, we used the collinear approximation for the photon momentum $q \to (1-z)p$ in the energy-momentum conserving δ-function and combined the reduced matrix element, the δ-function, $[{\rm d}p_Y]$ etc. into a differential cross section for the process $e + X \to Y$ where the four-momentum of the incoming electron is zp. To proceed further, we need to write the integration measure $[{\rm d}q]$ in Eq.(126) in a convenient way. It is easy to see that the following formula holds in the collinear $\theta_\gamma \to 0$ limit

$$\frac{{\rm d}^3q}{(2\pi)^3 2q_0}\frac{-2e^2}{(p-q)^2} = \frac{\alpha}{2\pi}\frac{{\rm d}q_\perp^2}{q_\perp^2}\,{\rm d}z. \tag{127}$$

Using this result in Eq. (126), we derive the forward photon emission contribution to the cross section of the process $e + X \to \gamma + Y$

$${\rm d}\sigma_{e+X\to\gamma+Y} = \frac{\alpha}{2\pi}\int_0^1 {\rm d}z\,\frac{1+z^2}{1-z}\int\frac{{\rm d}q_\perp^2}{q_\perp^2}\,{\rm d}\sigma(e(zp)+X\to Y). \tag{128}$$

There are three problems with the cross section formula shown in Eq. (128). The first problem is that integration over z diverges at $z = 1$. The second problem is that integration over $q_\perp$ appears to be unrestricted from above. The third problem is that integration over $q_\perp$ diverges at $q_\perp = 0$.

It is easy to understand that the two last problems are, essentially, self-inflicted. Indeed, a divergence at large values of $q_\perp$ is related to the approximate treatment of the phase space that was justified because $q_\perp$ was considered small, $q_\perp \ll \sqrt{s}$. Therefore, with the logarithmic accuracy, integration over $q_\perp$ should be cut at some value $q_\perp = q_{\perp,\max} \sim \sqrt{s}$. The exact value of $q_{\perp,\max}$ is, at this point, impossible to determine but since the dependence on this parameter is logarithmic and, therefore, weak, we do not need to be careful about it. Since, parametrically, $q_{\perp,\max}$ is of the order of the center of mass energy of the collision, we will use $q_{\perp,\max} = \sqrt{s}$ in what follows. Physically, it corresponds to the largest transverse momentum of the photon that we believe can still be be treated in the collinear approximation. Similarly, the divergence at small $q_\perp$ is related to our treatment of an incoming electron as a massless particle. This approximation is only justified for $q_\perp \gg m_e$ and, therefore, we should cut the integration over $q_\perp$ from below at $q_\perp \sim m_e$. Again, the *exact* value of the lower integration boundary is not important if we are content with the logarithmic accuracy of the calculation.

The divergence at $z = 1$ is more subtle. Since $q \approx (1-z)p$, $z \to 1$ corresponds to a situation where a *soft* photon is emitted. As we know from the discussion of the NLO computations, the emission of soft photons is indeed divergent and the divergence is canceled by the virtual corrections. The virtual corrections corresponds to elastic scattering process and, therefore, reside at $z = 1$. We can regulate the real emission contribution and introduce virtual corrections by writing the *inclusive* production cross section for the particle Y in the following way

$$\mathrm{d}\sigma^{\mathrm{incl}}_{e+X\to Y} = \int\limits_0^1 \mathrm{d}z \;\; \mathrm{d}\sigma(e(zp) + X \to Y)\; f_{e/e}(z,s), \tag{129}$$

where

$$f_{e/e}(z,s) = \delta(1-z) + \frac{\alpha}{2\pi}\left(\left[\frac{1+z^2}{1-z}\right]_+ + V\delta(1-z)\right)\log\frac{s}{m_e^2}. \tag{130}$$

Note that the structure of Eq. (129) is analogous to what we do in hadron collider physics when we compute hadronic cross sections by convoluting parton distributions with partonic cross sections. We therefore interpret $f_{e/e}(z,s)$ as the distribution of an "electron parton" in an original physical electron generated by the (real and virtual) emissions of collinear photons. Note that similar to parton distribution functions, the function $f_{e/e}(z,s)$ has two arguments: the first argument describes the energy fraction of the incoming electron carried by a parton, the second argument refers to an upper boundary imposed on $q_\perp$ integration which, effectively, corresponds to a definition of the kinematic region where collinear description of the final state is considered to be sensible.

We expect that collinear photon emissions generate a non-trivial energy spectrum of the "electron partons", but the number of electrons remains unchanged. This implies

$$\int\limits_0^1 \mathrm{d}z\; f_{e/e}(z,s) = 1 \quad \Rightarrow \quad f_{e/e}(z,s) = \delta(1-z) + \frac{\alpha}{2\pi}\left[\frac{1+z^2}{1-z}\right]_+ \ln\frac{s}{m_e^2}. \tag{131}$$

Note that the "electron number conservation" condition allows us to fix virtual corrections without computing them. The plus-distribution that multiplies the logarithm $\ln s/m_e^2$ is the electron splitting function

$$P_{ee} = \left[\frac{1+z^2}{1-z}\right]_+ = 2D_0(z) - (1+z) + \frac{3}{2}\delta(1-z). \tag{132}$$

Note that, up to a color factor, it coincides with the quark splitting function $P^{(0)}_{qq}$ discussed in Section 3.

The electron distribution function Eq. (131) has a number of important properties. If the collision energy is small $s \sim m_e^2$, the electron PDF reads $f_{e/e}(z, m_e^2) = \delta(1-z)$. This implies that collinear

emissions at low energies do not happen often. If, on the other hand, $s \gg m_e^2$, $f_{e/e}(z,s)$ becomes very sensitive to additional radiation since corrections to the elastic piece are controlled by the parameter $\alpha/\pi \log(s/m_e^2)$ and not by the fine structure constant α. Although in QED this parameter becomes close to one at inconceivably large energies, in QCD this happens earlier, which implies that the resummation of these logarithmically enhanced terms needs to be carried out. We will return to this point shortly.

We have discussed the process $e+X \to \gamma+Y$ in the collinear approximation. However, it is also possible to consider a process $e+X \to e+Y$ which corresponds to $\gamma+X \to Y$ elastic process. Working in the collinear approximation for that process, one can define a distribution function of a *photon parton* in the physical electron. The corresponding function reads

$$f_{e/\gamma}(z,s) = \frac{\alpha}{2\pi} \frac{1+(1-z)^2}{z} \ln \frac{s}{m_e^2}. \tag{133}$$

Note that $f_{e/\gamma}(z, m_e^2) = 0$, i.e. there are no photons in an electron if the radiation is suppressed.

It is instructive to compute the average momentum carried by the photon and electron constituents in a physical electron. Since the two distribution functions originate from the same splitting $e \to e+\gamma$ with the only difference that in one case we tag an electron and in the other case a photon, we expect that the average momenta carried by a photon and by an electron sum up to the momentum of the incoming electron. Clearly, this is true in every individual splitting and, therefore, it should be true on average. Performing explicit computation of the energy fractions

$$\langle z \rangle_e = \int\limits_0^1 \mathrm{d}z\; f_{e/e}(z,s)\; z = 1 - \frac{2\alpha}{3\pi} \ln \frac{s}{m_e^2}, \quad \langle z \rangle_\gamma = \int\limits_0^1 \mathrm{d}z\; f_{\gamma/e}(z,s)\; z = \frac{2\alpha}{3\pi} \ln \frac{s}{m_e^2}, \tag{134}$$

we find

$$\langle z \rangle_e + \langle z \rangle_\gamma = 1, \tag{135}$$

in agreement with the expectations.

We would like to generalize these results to the case when multiple photons are emitted; we will start with the case of two photons. There are two diagrams that contribute in this case and a $1/2!$ factor in the phase space that is necessary to include because photons are identical particles. The two diagrams differ by order in which photons are emitted off the incoming electron line. We note that these diagrams change the production cross section by an amount proportional to $\mathcal{O}(\alpha^2)$. Since we are only interested in contributions where each power of α is accompanied by a large logarithm $\ln(s/m_e^2)$, we need to understand how these diagrams can generate two powers of $\ln(s/m_e^2)$.

To see this, it is sufficient to compare propagators of an electron after the first and the second emissions. Consider a diagram where electron emits a photon with momentum q_1 and then a photon with momentum q_2. Electron propagator after the first emission scales as $1/q_{1,\perp}^2$, so that integration over $q_{1,\perp}$ is already logarithmic. The integration over $q_{2,\perp}$ can only be logarithmic if $q_{1,\perp} \ll q_{2,\perp}$ so that $q_{1,\perp}$ can be neglected in the electron propagator after the second emission. Clearly, everything that has just been said applies also to the second diagram – where electron first emits a photon with momentum q_2 and then the photon with momentum q_1 – after the replacement $q_1 \leftrightarrow q_2$. Hence, to account for *both diagrams*, we can take the contribution of the first one and remove the $1/2!$ symmetry factor from the phase space.

The constraints on the transverse momenta of the emitted photons define integration regions over $q_\perp$ that lead to the double-logarithmic enhancement of these $\mathcal{O}(\alpha^2)$ contributions. Since the transverse momentum ordering described above implies sequential approach of the collinear limits, it is clear that the Sudakov decomposition of the second emission needs to be performed relative to the electron four-momentum *after* the emission of the first photon, i.e.

$$q_1 = (1-z_1)p + ..., \qquad q_2 = (1-z_2)z_1 p + ... \tag{136}$$

Generalizing this discussion to arbitrary number of photons and neglecting the possibility that an electron fluctuates into a virtual photon, we obtain the following result for the inclusive cross section

$$\sigma_{e+X\to Y+\text{anything}} = \int\limits_0^1 \mathrm{d}z\; f_{e/e}(z,s)\; \mathrm{d}\sigma(e(zp)+X\to Y). \tag{137}$$

where

$$\begin{aligned} f_{e/e}(z,s) = \delta(1-z) + \sum_{n=1}^{\infty}\left(\frac{\alpha}{2\pi}\right)^n \int\limits_0^1 \mathrm{d}z_n P_{ee}(z_n) \int\limits_{m_e^2}^{s} \frac{\mathrm{d}q_{n,\perp}^2}{q_{n,\perp}^2} \times \\ \int\limits_0^1 \mathrm{d}z_{n-1} P_{ee}(z_{n-1}) \int\limits_{m_e^2}^{q_{n,\perp}^2} \frac{\mathrm{d}q_{n-1,\perp}^2}{q_{n-1,\perp}^2} \times \cdots \times \int\limits_0^1 \mathrm{d}z_1 P_{ee}(z_1) \int\limits_{m_e^2}^{q_{2,\perp}^2} \frac{\mathrm{d}q_{1,\perp}^2}{q_{1,\perp}^2}\; \delta(z_1 ... z_n - z). \end{aligned} \tag{138}$$

This expression appears to be relatively complicated. However, we can re-write it in a more compact form by computing logarithmic derivative of $f_{e/e}(s,z)$ with respect to s. Recall that $\sqrt{s}$ represents the largest value of the transverse momentum of an emitted photon that we agree to treat in the collinear approximation.

It is straightforward to compute the derivative since s appears only as an upper boundary of the left-most integral over $p_\perp$ in each term in Eq. (138). We obtain

$$s\frac{\partial f_{e/e}(z,s)}{\partial s} = \frac{\alpha}{2\pi}\int\limits_0^1 \mathrm{d}z_1 P_{ee}(z_1) \left[\delta(z-z_1) + \frac{\alpha}{2\pi}\int\limits_0^1 \mathrm{d}z_2 P_{ee}(z_2) \int\limits_{m_e^2}^{s} \frac{\mathrm{d}q_{2,\perp}^2}{q_{2,\perp}^2}\delta(z-z_1 z_2) + \cdots\right]. \tag{139}$$

We can cast the right-hand side of this equation into a more recognizable expression by removing z_1 from all δ-functions that appear in square brackets in Eq. (139). We use the identity

$$\delta(z - z_1 \cdots) = \frac{1}{z_1}\delta(z/z_1 - \cdots), \tag{140}$$

and realize that the expression in square brackets in Eq. (139) can be identified with $1/z_1 f_{e/e}(z/z_1, s)$. Hence, the differential equation Eq. (139) becomes

$$s\frac{\partial f_{e/e}(z,s)}{\partial s} = \frac{\alpha}{2\pi}\int\limits_0^1 \frac{\mathrm{d}z_1}{z_1} P_{ee}(z_1) f_{e/e}(z/z_1, s) = \int\limits_0^1 \mathrm{d}z_1 \mathrm{d}z_2 P_{ee}(z_1) f_{e/e}(z_2,s)\delta(z-z_1 z_2). \tag{141}$$

This is the QED version of the celebrated Dokshitzer-Gribov-Altarelli-Parisi (DGLAP) evolution equation [18]. We note that Eq. (141) is not complete since we neglected possible splittings of an electron to a photon or to a positron, but it gives us an idea of how the DGLAP equation looks like and how it appears.

The DGLAP equation can be solved provided that the distribution function is known for some value of s. In the QED case $s = m_e^2$ is special and $f_{e/e}(z, m_e^2) = \delta(1-z)$. We can find $f_{e/e}(z,s)$ for $s \neq m_e^2$ by solving the DGLAP equation Eq. (141).

We will now summarize what we have seen so far. Parton distribution functions naturally appear if we attempt to describe quasi-collinear emissions by colliding particles, including the *elementary ones*. These functions depend on two parameters – the fraction of energy of the incoming particle that a parton carries into a hard collision and the "factorization scale" which, roughly, corresponds to the

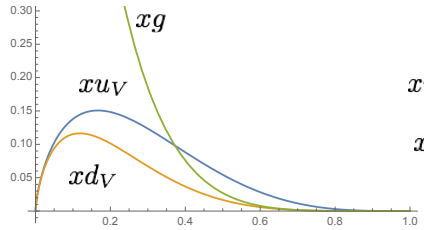

$$Q_0 = 3 \text{ GeV}$$

$$xu_V \sim x^{0.7}(1-x)^{3.5}, \quad xd_v \sim x^{0.7}(1-x)^{5.2}$$

$$xu_s \sim xd_s \sim x^{-0.2}(1-x)^{7}, \quad xg \sim x^{-0.2}(1-x)^{5.4}$$

Fig. 7: Typical proton parton distribution functions at the factorization scale 3 GeV.

maximal value of the transverse momentum that is considered acceptable to be treated in the collinear approximation and whose impact on final state kinematics is ignored. Although we have illustrated these points in the context of QED, they are valid in QCD as well. The most important difference between QED and QCD is that in QCD we do not know the initial condition for parton distribution functions at low factorization scale since QCD is non-perturbative and since we are mostly interested in parton distribution functions of non-elementary particles (protons, neutrons etc.). On the other hand, the QCD evolution equations are very similar to what we derived in QED, with obvious modifications to allow for transitions between different types of partons and the running of the coupling constant. The DGLAP equations in QCD read

$$\begin{aligned}
s\frac{\partial q_i(z,s)}{\partial s} &= \frac{\alpha_s(s)}{2\pi}\int\limits_0^1 \frac{\mathrm{d}\xi}{\xi}\Big[P_{q\to q}(\xi)q_i(\xi/z) + P_{\bar{q}\to q}(\xi)\bar{q}_i(z/\xi,s) \\
&\qquad + P_{q'\to q}(\xi)\sum_{j\neq i}\big(q_j(z/\xi,s)+\bar{q}_j(z/\xi,s)\big) + P_{g\to q}(\xi)\, g(z/\xi,s)\Big], \\
s\frac{\partial \bar{q}_i(z,s)}{\partial s} &= \frac{\alpha_s(s)}{2\pi}\int\limits_0^1 \frac{\mathrm{d}\xi}{\xi}\Big[P_{q\to q}(\xi)\bar{q}_i(\xi/z) + P_{\bar{q}\to q}(\xi)q_i(z/\xi,s) \\
&\qquad + P_{q'\to q}(\xi)\sum_{j\neq i}\big(q_j(z/\xi,s)+\bar{q}_j(z/\xi,s)\big) + P_{g\to q}(\xi)\, g(z/\xi,s)\Big], \\
s\frac{\partial g(z,s)}{\partial s} &= \frac{\alpha_s(s)}{2\pi}\int\limits_0^1 \frac{\mathrm{d}\xi}{\xi}\Big[P_{q\to g}(\xi)\sum\big(q_j(z/\xi,s)+\bar{q}_j(z/,\xi)\big) + P_{g\to g}(\xi)\, g(z/\xi,s)\Big].
\end{aligned} \tag{142}$$

The Altarelli-Parisi splitting functions in QCD are well-known. At leading order, all of them, except P_{gg}, can be obtained from the corresponding QED results. We present the leading order splitting functions here for completeness

$$\begin{aligned}
&P_{q\to q} = C_F\left[\frac{1+z^2}{1-z}\right]_+, \qquad P_{q\to g} = C_F\frac{1+(1-z)^2}{z}, \qquad P_{g\to q} = T_R(z^2+(1-z)^2), \\
&P_{g\to g} = 2C_A\left[\frac{1-z}{z} + \frac{z}{(1-z)_+} + z(1-z) + \left(\frac{11}{6}C_A - \frac{2n_f T_R}{3}\right)\delta(1-z)\right].
\end{aligned} \tag{143}$$

The DGLAP equations imply that parton distribution functions at any scale can be determined if they are known at some scale. So, the strategy is to parametrize parton distributions at a relatively low scale and then use the DGLAP evolution and various data to determine them. Typical results are shown in Fig. 7 where quarks are split into *valence* (constituent) and *sea* (produced by the gluon splitting)

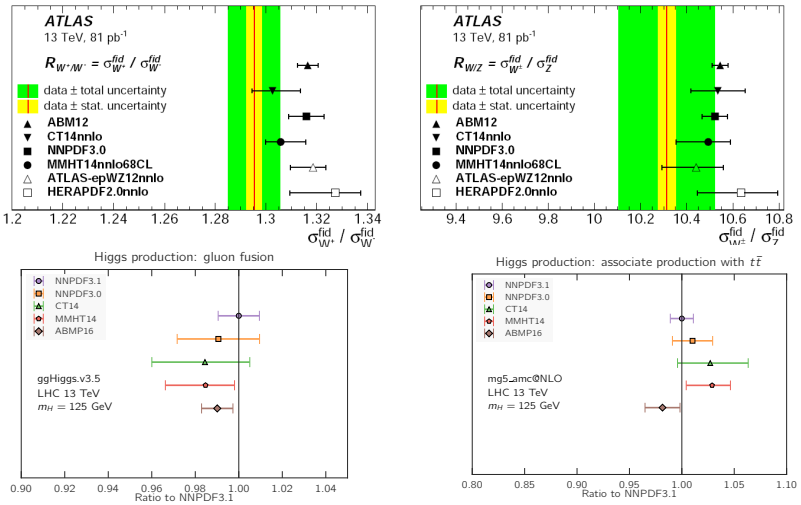

Fig. 8: Comparison of physical cross sections for a few selected processes computed with popular parton distribution functions.

contributions. Understanding uncertainties in the determination of parton distribution functions is an important question that is being constantly discussed and refined [25]. Another complication is that extraction of PDFs involves fixed order cross section computations. When fixed order results change (i.e. by accounting for higher order QCD corrections), the PDFs change as well (provided, of course, that data does not). It is therefore customary to extract PDFs employing fixed order cross sections of certain accuracy (LO, NLO, NNLO). These (LO, NLO, NNLO) PDFs sets should be used to predict physical observables using *matching orders* in computed partonic cross sections.

How well do we know parton distributions functions? A snapshot of the current situation is shown in Fig. 8 for a variety of Standard Model processes including $pp \to V$ with $V = W, Z$, $pp \to H$ and $pp \to t\bar{t}H$. We see that different PDF sets are in reasonable agreement and, at this point, there are no PDF sets that are in a clear disagreement with the other sets. This is quite encouraging and suggests that, with sufficient effort, parton distribution functions can be understood well-enough to allow for the precision physics program at the LHC.

7 Parton showers

Parton distribution functions provide limited information about final state particles. Indeed, to derive the DGLAP evolution equation, we integrate over momenta of the emitted particles loosing information about kinematics of the final state. This may not be ideal since, in certain cases, we may want to have a more detailed description of the final states. This can be done with the help of the so-called *parton shower programs*. The most famous examples of such programs are PYTHIA, HERWIG and SHERPA [26] whose relevance for experiments in high-energy physics is hard to overstate. The goal of this Section is to introduce basic ideas behind parton showers and explain how they can be used to simulate unweighted events.

7.1 The toy model

Following the spirit of the previous Sections, we will start the discussion of parton showers with a toy model inspired by soft emissions in QED. As we have already mentioned in these Lectures, soft emissions in QED completely factorize, c.f. Eq. (105). The cross section in the soft photon approximation is obtained by integrating over photon energies with an additional constraint that the total radiated en-

ergy and the energy that remains in the radiator E can not exceed the total energy available before the emissions. We write

$$\mathrm{d}\sigma_n = \frac{\alpha^n}{n!}\,\mathrm{d}\sigma_0\,\mathrm{d}E\,\prod_{i=1}^{n}\frac{\mathrm{d}\omega_i}{\omega_i}\,\delta(E_T - E - \sum_{i=1}^{n}\omega_i). \tag{144}$$

We integrate over the energy E of the radiator and find

$$\mathrm{d}\sigma_n = \frac{\alpha^n}{n!}\,\mathrm{d}\sigma_0\,\prod_{i=1}^{n}\frac{\mathrm{d}\omega_i}{\omega_i}\,\theta(E_T - \sum\omega_i). \tag{145}$$

Solving the θ-function constraint and introducing a lower integration boundary for integration over ω, we write

$$\mathrm{d}\sigma_n = \frac{\alpha^n}{n!}\mathrm{d}\sigma_0\int\limits_{\lambda}^{E_T}\frac{\mathrm{d}\omega_1}{\omega_1}\int\limits_{\lambda}^{E_T-\omega_1}\frac{\mathrm{d}\omega_2}{\omega_2}\int\limits_{\lambda}^{E_T-\omega_1-\omega_2}\frac{\mathrm{d}\omega_3}{\omega_3}\cdots\int\limits_{\lambda}^{E_T-\omega_1-\omega_2-\cdots-\omega_{n-1}}\frac{\mathrm{d}\omega_n}{\omega_n}. \tag{146}$$

The cross section σ_n is a function of E_T/λ; we would like to evaluate this function in the limit $\lambda \to 0$ which corresponds to $E_T/\lambda \to \infty$. We will now show that, in order to pick up the largest logarithmic contribution to the integral $\mathrm{d}\sigma_n$, we can neglect all dependencies on energies in integration boundaries in Eq. (146)

$$\int\limits_{\lambda}^{E_T}\frac{\mathrm{d}\omega_1}{\omega_1}\int\limits_{\lambda}^{E_T-\omega_1}\frac{\mathrm{d}\omega_2}{\omega_2}\int\limits_{\lambda}^{E_T-\omega_1-\omega_2}\frac{\mathrm{d}\omega_3}{\omega_3}\cdots \to \int\limits_{\lambda}^{E_T}\frac{\mathrm{d}\omega_1}{\omega_1}\int\limits_{\lambda}^{E_T}\frac{\mathrm{d}\omega_2}{\omega_2}\int\limits_{\lambda}^{E_T}\frac{\mathrm{d}\omega_3}{\omega_3}\cdots = \log^n\frac{E_T}{\lambda}. \tag{147}$$

To illustrate why this approximation gives the correct *highest* power of a large logarithm, we consider the case of the two emissions and compute

$$\begin{aligned} I_2 &= \int\limits_{\lambda}^{E_T}\frac{\mathrm{d}\omega_1}{\omega_1}\int\limits_{\lambda}^{E_T-\omega_1}\frac{\mathrm{d}\omega_2}{\omega_2} = \int\limits_{\lambda}^{E_T}\frac{\mathrm{d}\omega_1}{\omega_1}\log\frac{E_T-\omega_1}{\lambda} \\ &= \int\limits_{\lambda}^{E_T}\frac{\mathrm{d}\omega_1}{\omega_1}\left[\ln\frac{E_T}{\lambda} + \ln\left(1-\frac{\omega}{E_T}\right)\right] = \ln^2\frac{E_T}{\lambda} + \int\limits_{\lambda}^{E_T}\frac{\mathrm{d}\omega_1}{\omega_1}\ln\left(1-\frac{\omega_1}{E_T}\right) \end{aligned} \tag{148}$$

Note that the last integral is convergent in the $\omega_1 \to 0$ limit, so that the dependence on λ can be neglected. Upon doing that and changing integration variables $\omega_1 = E_T\xi$, we arrive at

$$I_2 \approx \ln^2\frac{E_T}{\lambda} + \int\limits_0^1\frac{\mathrm{d}\xi}{\xi}\ln(1-\xi) = \ln^2\frac{E_T}{\lambda} - \frac{\pi^2}{6} \approx \ln^2\frac{E_T}{\lambda}, \tag{149}$$

where in the last step we neglected the constant term. Clearly, the logarithmically-enhanced term can be obtained if we neglect the dependence of the integration boundaries on the photon energy

$$I_2 = \int\limits_{\lambda}^{E_T}\frac{\mathrm{d}\omega_1}{\omega_1}\int\limits_{\lambda}^{E_T-\omega_1}\frac{\mathrm{d}\omega_2}{\omega_2} \approx \int\limits_{\lambda}^{E_T}\frac{\mathrm{d}\omega_1}{\omega_1}\int\limits_{\lambda}^{E_T}\frac{\mathrm{d}\omega_2}{\omega_2} = \ln^2\frac{E_T}{\lambda}. \tag{150}$$

The generalization to the case of a larger number of photons is obvious. We conclude that, with the leading logarithmic accuracy, the cross section for producing n photons reads

$$\mathrm{d}\sigma_n \approx \frac{\alpha^n}{n!}\sigma_0\ln^n\frac{E_T}{\lambda}. \tag{151}$$

The cross section for emitting *any* number of photons is obtained by summing Eq. (151) over n. We obtain

$$\mathrm{d}\sigma = \sum_0^\infty \mathrm{d}\sigma_n = \mathrm{d}\sigma_0 \; e^{\alpha \ln \frac{E_T}{\lambda}}. \tag{152}$$

The result shown in Eq. (152) is rather strange since it implies that soft emissions make the cross section very large. We know from previous discussions that this can only happen if *virtual* corrections are improperly neglected and, if real and virtual corrections are combined, no logarithmically enhanced corrections appear in the cross section integrated over all soft emissions. Since we work with the logarithmic accuracy, we have to find

$$\mathrm{d}\sigma_{\text{full}} = \mathrm{d}\sigma_0, \tag{153}$$

in variance with Eq. (152).

To account for virtual corrections we write, in accord with Eq. (153),

$$\mathrm{d}\sigma_{\text{full}} = \mathrm{d}\sigma_0 V e^{\alpha \ln E_T/\lambda}, \tag{154}$$

where $V = e^{-\alpha \ln E_T/\lambda}$ represents the effect of virtual corrections. We can now expand the real emission exponential back and find

$$1 = \sum_{n=0}^\infty P_n, \tag{155}$$

where

$$P_n = e^{-\alpha \ln E_T/\lambda} \; \alpha^n \int\limits_\lambda^{E_T} \frac{\mathrm{d}\omega_1}{\omega_1} \int\limits_\lambda^{\omega_1} \frac{\mathrm{d}\omega_2}{\omega_2} \int\limits_\lambda^{\omega_2} \frac{\mathrm{d}\omega_3}{\omega_3} \cdots \int\limits_\lambda^{\omega_{n-1}} \frac{\mathrm{d}\omega_n}{\omega_n}. \tag{156}$$

We interpret the different contributions in Eq. (155) as the relative probabilities to produce a final state with *certain number of photons*. Integrations over ω's in Eq. (156) represent sampling over different kinematic configurations that contribute to these final states. Our goal is to turn Eqs. (155,156) into a generator of *unweighted events* where, similar to experimental reality, each event is characterized by a collection of photons with definite energies.

To proceed further, we introduce a notation $\phi(x,y) = \alpha \ln x/y$, write

$$e^{-\alpha \ln E_T/\lambda} = e^{-\phi(E_T,\omega_1)} e^{-\phi(\omega_1,\omega_2)} ... e^{-\phi(\omega_{n-1},\omega_n)} e^{-\phi(\omega_n,\lambda)}, \tag{157}$$

and insert this representation into the integral in Eq. (156). We obtain

$$\mathcal{P}_n = \alpha^n \int\limits_\lambda^{E_T} \frac{\mathrm{d}\omega_1}{\omega_1} e^{-\phi(E_T,\omega_1)} \int\limits_\lambda^{\omega_1} \frac{\mathrm{d}\omega_2}{\omega_2} e^{-\phi(\omega_1,\omega_2)} .. \int\limits_\lambda^{\omega_{n-1}} \frac{\mathrm{d}\omega_n}{\omega_n} e^{-\phi(\omega_{n-1},\omega_n)} e^{-\phi(\omega_n,\lambda)} \tag{158}$$

We then change variables $\omega_i \to r_i = e^{-\phi(\omega_{i-1},\omega_i)}$, find the Jacobians of the variable transformations and the new integration boundaries

$$\mathrm{d}r_i = \alpha \frac{\mathrm{d}\omega_i}{\omega_i} e^{-\phi(\omega_{i-1},\omega_i)}, \qquad r_{\min}(\omega_{i-1}) < r_i < 1, \quad r_{\min}(\omega) = e^{-\alpha \ln \omega/\lambda}. \tag{159}$$

We then write $\mathcal{P}_n$ using new variables

$$\mathcal{P}_n = \int\limits_{r^{\min}(\omega_0)}^1 \mathrm{d}r_1 \int\limits_{r^{\min}(\omega_1)}^1 \mathrm{d}r_2 .. \int\limits_{r^{\min}(\omega_{n-1})}^1 \mathrm{d}r_n \; e^{-\phi(\omega_n,\lambda)}, \tag{160}$$

where $\omega_0 = E_T$.

It is instructive to compute the probability to emit $n + X$ photons, where X is an arbitrary final state. This probability is given by

$$\begin{aligned}\mathcal{P}_{n+X} = &\int\limits_{r^{\min}(\omega_0)}^{1} \mathrm{d}r_1 \int\limits_{r^{\rm in}(\omega_1)}^{1} \mathrm{d}r_2 .. \int\limits_{r^{\min}(\omega_{n-1})}^{1} \mathrm{d}r_n \\ &\times \left[e^{-\phi(\omega_n,\lambda)} + \int\limits_{r^{\min}(\omega_n)}^{1} \mathrm{d}r_{n+1} e^{-\phi(\omega_{n+1},\lambda)} + \int\limits_{r^{\min}(\omega_n)}^{1} \mathrm{d}r_{n+1} \int\limits_{r^{\min}(\omega_{n+1})}^{1} \mathrm{d}r_{n+2} e^{-\phi(\omega_{n+2},\lambda)} + \cdots \right] \\ = &\int\limits_{r^{\min}(\omega_0)}^{1} \mathrm{d}r_1 \int\limits_{r^{\rm in}(\omega_1)}^{1} \mathrm{d}r_2 .. \int\limits_{r^{\min}(\omega_{n-1})}^{1} \mathrm{d}r_n,\end{aligned} \tag{161}$$

where in the last step we used the fact that the expression in square brackets is the total probability to produce *any* final state which isi equal to one.

The formula Eq. (161) suggests how events can be generated since the probability to emit a photon with particular energy is independent of whether or not subsequent emissions occur. The first step is to decide if at least one emission happened. The probability for at least one emission is given by

$$\mathcal{P}_1 = \int\limits_{r^{\min}(E_T)}^{1} \mathrm{d}r_1. \tag{162}$$

The probability that event contains no (resolved) emissions is given by $\mathcal{P}_0 = r^{\min}(E_T) = 1 - \mathcal{P}_1$.

To produce events with these probability distributions, we generate a random number with the flat probability distribution $0 < \xi_1 < 1$. If $\xi_1 < P_0$, no emission happened. We exit the generation process and register an event which contains *no photon emissions*. To generate *another* event, we return to the beginning of the generation process.

If, on the other hand, $\mathcal{P}_0 < \xi_1 < 1$, the photon emission did happen. We find the energy of the emitted photon by solving the equation $\xi_1 = e^{-\phi(\omega_0,\omega_1)}$ for ω_1. The result reads $\omega_1 = \omega_0 \xi_1^{1/\alpha}$. Next, we need to determine if the second photon is emitted. We repeat the first step with the only difference that we use ω_1 instead of E_T to compute the no-emission probability. For example, if the second emission does happen, the energy of the second photon reads $\omega_2 = \omega_1 \xi_2^{1/\alpha}$.

Clearly, we can keep doing that until a no-emission event is generated. Note that the probability to generate a no-emission event grows because energies of the radiated photons decrease as we generate more and more photons. Once the energy of the emitted photon becomes comparable to λ, the no-emission probability becomes close to one and the generation process has a high chance to terminate. At any rate, once the no-emission event is generated, we exit the event generation process. At this point, we have the list of photons with their energies; this list provides complete kinematic description of the generated event. If we need to generate another event, we start from the beginning. One can work with these unweighted events in the same way experimentalists work with real events recorded in experiments at the LHC and compute the relevant cross sections and distributions simply by combining them in an appropriate way.

The above procedure gives us a toy model of a parton shower. It shows that parton showers develop an approximate treatment of perturbative corrections to cross sections and distribution by picking up the

logarithmically enhanced terms, treating the radiation phase space in a simplified manner and preserving hard cross sections by requiring that integrated real emission and virtual corrections cancel each other exactly. This last feature allows us to define a "conserved quantity" that we then recast into a *probability* and use it to generate events with particular kinematic features of final state particles.

7.2 Parton shower description of collinear emissions

We would like to move beyond the toy model and develop a parton shower description of a gauge theory. We will again start with QED and make use of our discussion of parton distribution functions. To develop the probabilistic picture, inherent to parton showers, we need to understand what can play a role of a conserved quantity in case of collinear emissions. To this end, recall that an electron distribution in a physical electron satisfies the DGLAP evolution equation

$$s\frac{\partial}{\partial s}f_{e/e}(z,s)=\frac{\alpha}{2\pi}\int\limits_0^1 \mathrm{d}z_1\mathrm{d}z_2 P_{ee}(z_1)f_{e/e}(z_2,s)\delta(z-z_1z_2). \tag{163}$$

We integrate both sides of this equation over z and find

$$s\frac{\partial}{\partial s}\int\limits_0^1 \mathrm{d}z\; f_{e/e}(z,s)=\int\limits_0^1 \mathrm{d}z_1 P_{ee}(z_1)\int\limits_0^1 \mathrm{d}z_2 f_{e/e}(z_2)=0, \tag{164}$$

where the last step follows from the fact that $P_{ee}(z)$ is a plus-distribution, c.f. Eq. (132).

The above equation implies that the *integral* of $f_{e/e}(z,s)$ over z is independent of s and since $f_{e/e}(z,m_e^2)=\delta(1-z)$, we find

$$\int\limits_0^1 \mathrm{d}z f_{e/e}(z,s)=1. \tag{165}$$

We would like to interpret Eq. (165) as a probability conservation condition that will allow us to compute the relative probabilities of collinear photon emissions. To this end, we re-write the DGLAP equation by separating real and virtual corrections in the splitting function

$$s\frac{\partial}{\partial s}f_{e/e}(z,s)=\frac{\alpha}{2\pi}\int\limits_0^1 \mathrm{d}\xi\tilde{P}_{ee}(\xi)\left[\frac{f_{e/e}(z/\xi,s)}{\xi}-f_{e/e}(z,s)\right], \tag{166}$$

where $\tilde{P}_{ee}(\xi)=(1+\xi^2)/(1-\xi)$. We would like to treat the two terms on the right hand side of Eq. (166) separately; to do that we need to introduce a cut-off on the integration over ξ, $\xi<1-\delta$. After moving $f_{e/e}(z,s)$ to the left hand side of Eq.(166), we obtain

$$s\frac{\partial}{\partial s}f_{e/e}(z,s)+\frac{\alpha}{2\pi}\left[\int\limits_0^{1-\delta}\mathrm{d}\xi\;\tilde{P}_{ee}(\xi)\right]f_{e/e}(z,s)=\int\limits_0^{1-\delta}\frac{\mathrm{d}\xi}{\xi}\tilde{P}_{ee}(\xi)f_{e/e}(\frac{z}{\xi},s). \tag{167}$$

We will solve Eq.(167) in the approximation $\delta\to 0$. Note that the singularity at $\xi=0$ is irrelevant since it is protected by the fact that the splitting function vanishes for values of arguments that are bigger than one. To solve Eq. (167), we remove the homogeneous part of the equation by writing

$$f_{e/e}(z,s)=\Delta(s)g(z,s), \tag{168}$$

and choose $\Delta(s)$ to satisfy the differential equation

$$s\frac{\partial}{\partial s}\Delta(s)+\frac{\alpha}{2\pi}\left[\int\limits_0^{1-\delta}\mathrm{d}\xi\ \tilde{P}_{ee}(\xi)\right]\Delta(s)=0. \tag{169}$$

The equation for $g(z,s)$ becomes

$$s\frac{\partial g(z,s)}{\partial s}=\frac{\alpha}{2\pi}\int\limits_0^{1-\delta}\frac{\mathrm{d}\xi}{\xi}\tilde{P}_{ee}(\xi)g(z/\xi,s). \tag{170}$$

To find the splitting function $f_{e/e}(z,s)$ we need to solve the differential equations Eqs. (169,170). We begin with Eq. (169). Its solution reads

$$\Delta(s,m_e^2)=\exp\left[-\frac{\alpha}{2\pi}\int\limits_{m_e^2}^{s}\frac{\mathrm{d}t}{t}\int\limits_0^{1-\delta}\mathrm{d}\xi\tilde{P}_{ee}(\xi)\right]. \tag{171}$$

We note that $\Delta(s,m_e^2)$ is known as the *Sudakov form factor*. As we will see later, it describes a probability of the elastic (no-emission) process.

We integrate Eq. (170) over s and find

$$g(z,s)=g(z,m_e^2)+\frac{\alpha}{2\pi}\int\limits_{m_e^2}^{s}\frac{\mathrm{d}t}{t}\int\limits_0^{1-\delta}\frac{\mathrm{d}\xi}{\xi}\tilde{P}_{ee}(\xi)g(z/\xi,t). \tag{172}$$

If we multiply both sides of this equation with $\Delta(s,m_e^2)$ and use the fact that $\Delta(m_e^2,m_e^2)=1$, we obtain

$$f_{e/e}(z,s)=\Delta(s,m_e^2)f_{e/e}(z,m_e^2)+\frac{\alpha}{2\pi}\int\limits_{m_e^2}^{s}\frac{\mathrm{d}t}{t}\Delta(s,t)\int\limits_0^{1-\xi_{\min}}\frac{\mathrm{d}\xi}{\xi}\ \tilde{P}_{ee}(\xi)\ f_{e/e}(z/\xi,t). \tag{173}$$

We can expand the right hand side of Eq. (173) in power series in α, treating the Sudakov form factor as quantity of order one and using $f_{e/e}(z,m_e^2)=\delta(1-z)$. This is very similar to what we did when constructing the probability conservation equation in the toy model. We obtain

$$\begin{aligned}f_{e/e}(s,z)&=\Delta(s,m_e^2)\delta(1-z)+\frac{\alpha}{2\pi}\int\limits_{m_e^2}^{s}\frac{\mathrm{d}t_1}{t_1}\Delta(s,t_1)\int\limits_0^{1-\delta}\mathrm{d}\xi_1\tilde{P}_{ee}(\xi_1)\Delta(t_1,m_e^2)\delta(z-\xi_1)\\&+\left(\frac{\alpha}{2\pi}\right)^2\int\limits_{m_e^2}^{s}\frac{\mathrm{d}t_1}{t_1}\Delta(s,t_1)\int\limits_0^{1-\delta}\mathrm{d}\xi_1\tilde{P}_{ee}(\xi_1)\int\limits_{m_e^2}^{t_1}\frac{\mathrm{d}t_2}{t_2}\Delta(t_1,t_2)\int\limits_0^{1-\delta}\mathrm{d}\xi_2\tilde{P}_{ee}(\xi_2)\Delta(t_2,m_e^2)\delta(z-\xi_1\xi_2)\\&+\cdots\end{aligned} \tag{174}$$

We now integrate both sides of Eq. (174) over z, use the "probability conservation" condition Eq. (165)

and obtain an equation that we can use to generate events in exactly the same way as in the toy model

$$\begin{aligned}1 &= \Delta(s,m_e^2) + \frac{\alpha}{2\pi}\int\limits_{m_e^2}^{s}\frac{\mathrm{d}t_1}{t_1}\Delta(s,t_1)\int\limits_0^{1-\delta}\mathrm{d}\xi_1\tilde{P}_{ee}(\xi_1)\Delta(t_1,m_e^2)\\ &+\left(\frac{\alpha}{2\pi}\right)^2\int\limits_{m_e^2}^{s}\frac{\mathrm{d}t_1}{t_1}\Delta(s,t_1)\int\limits_0^{1-\delta}\mathrm{d}\xi_1\tilde{P}_{ee}(\xi_1)\int\limits_{m_e^2}^{t_1}\frac{\mathrm{d}t_2}{t_2}\Delta(t_1,t_2)\int\limits_0^{1-\delta}\mathrm{d}\xi_2\tilde{P}_{ee}(\xi_2)\Delta(t_2,m_e^2)\\ &+\cdots\end{aligned} \tag{175}$$

Each term in these series represents a probability of a process with a fixed number of resolved photons. The generation process works similarly to the toy model. Note that this similarity can be made exact if, similar to the toy model, we introduce a random variable

$$r_i = \Delta(t_{i-1},t_i), \quad t_0 = s. \tag{176}$$

Indeed, since

$$\mathrm{d}r_i = \frac{\alpha}{2\pi}\frac{\mathrm{d}t_i}{t_i}\int\limits_0^{1-\delta}\mathrm{d}\xi_1\tilde{P}_{ee}(\xi_1)\;\Delta(t_{i-1},t_i), \tag{177}$$

Eq. (175) can be cast into a form that is identical to e.g. Eq. (161) discussed in the context of the toy model. Therefore, we can generate events following our earlier discussion. The only difference is that we need more than one random variables to describe momentum of an emitted photon.

We now explain the procedure in detail. We begin with generating a random number $0 < r < 1$ and solving the equation

$$\Delta(s,t_1) = r \tag{178}$$

for t_1. If $t_1 < m_e^2$, then no emission happens, we exit the generation process and, if necessary, start anew. If, on the other hand, we find $t_1 > m_e^2$, then the emission happens. To determine the energy of the photon, we generate another random variable $0 < y_1 < 1$ and solve for ξ_1

$$y_1 = \frac{\int\limits_0^{\xi_1}\mathrm{d}\bar{\xi}P_{ee}(\bar{\xi})}{\int\limits_0^{1-\delta}\mathrm{d}\bar{\xi}P_{ee}(\bar{\xi})}. \tag{179}$$

The two variables, ξ_1 and t_1 allow us to compute the four-momentum of the radiated photon

$$q_1^\mu = (1-\xi_1)p^\mu + \beta_1\bar{p}^\mu + q_{\perp,1}n_{\perp,1}^\mu, \tag{180}$$

where $q_{\perp,1} = \sqrt{t_1}$, $n_{\perp,1}^\mu$ is a randomly generated unit vector, $n_{\perp,1}^2 = -1$, in a plane transverse to p and $\bar{p}$ and $\beta_1 = t_1/((1-\xi_1)2p\bar{p})$.

Once the photon is generated, the next step is repeated with s replaced by t_1. This means that we again generate a random number $0 < r < 1$ and solve the equation

$$r = \Delta(t_1,t_2) \tag{181}$$

for t_2. If we find that $t_2 < m_e^2$, we declare that no further photon emission happened and we exit the generation process. If, on the other hand, $t_2 > m_e^2$, we generate abother random variable y_2, determine ξ_2 from an analog of Eq. (179) and compute the momentum of the second emitted photon as

$$q_2^\mu = (1-\xi_2)\xi_1 p^\mu + \beta_2\bar{p}^\mu + q_{\perp,2}n_{\perp,2}^\mu, \tag{182}$$

where $q_{\perp,2} = \sqrt{t_2}$ etc. This process continues unless at some stage the no-emission event is generated. If this happens, we exit the generation process. At this point we have a list of photon momenta that describes an event – with fully specified final state – for the process $e + X \to Y + \text{photons}$ in the collinear approximation for the emitted photons.

The generalization to QCD is, in principle, straightforward since the above discussion is built around the analysis of the DGLAP evolution equation for the structure functions. One can repeat all the steps almost verbatim and arrive at a similar conclusion. One aspect that, in principle, one should also consider in QED, is a possibility to split into different types of partons. Indeed, in QCD all different types of branchings $a \to b + c$ have to be taken into account. As the result, there are different Sudakov form factor for different partons and a sum over all types of possible branchings appears in the exponent. The other aspect that we have been systematically neglecting in our QED discussion is the running of the coupling constant that definitely has to be accounted for in QCD. The Sudakov form factor of a parton a reads

$$\Delta_a(s, s_0) = \exp\left[\int\limits_{s_0}^{s} \frac{\mathrm{d}t}{t}\frac{\alpha_s(t)}{2\pi}\int\limits_0^{1-\delta}\mathrm{d}\xi \sum_b P_{a\to b}(\xi)\right]. \tag{183}$$

We generate events in exactly the same way as discussed above except that at every step we need to decide which branching actually happens. This is done based on the relative probabilities for individual branchings

$$w_{a\to b} = \frac{\int\limits_0^{1-\delta}\mathrm{d}\xi P_{a\to b}(\xi)}{\int\limits_0^{1-\delta}\mathrm{d}\xi \sum\limits_b P_{a\to b}(\xi)}. \tag{184}$$

7.3 Soft emissions and parton showers

We have discussed how to generate events that describe emissions of collinear partons from initial state particles. Note that since we generate collinear emissions and since collinear emissions from different particles do not interfere, it becomes straightforward to generalize our discussion to an arbitrary number of incoming and outgoing particles. However, we have also seen in the computation of NLO QCD corrections that infra-red divergences – and related logarithmically-enhanced contributions – can have either collinear or *soft* origin. The construction of a parton shower that we described addresses collinear singularities and large collinear logarithms. However, if soft contributions are to play an important role, how can they be accommodated into this framework?

The important difference between soft and collinear emissions is that soft gluons emitted by different color charges necessarily interfere so that emission of soft gluons does not occur locally in the phase space – it requires a snapshot of the whole system. This is very different from independent collinear emissions and it is unclear a priori if the parton shower framework can accommodate soft emissions.

It turns out that it is actually possible to describe soft emissions with parton showers. In fact, there are at least *two* ways to do that; I will explain below the classic one [7] based on the concept of the so-called *angular ordering*.[6] To understand what this is, consider a soft photon emission from an electron-positron pair that is produced in the splitting of a virtual photon $\gamma^* \to e^+e^-$. We know that the full matrix element squared is given by the eikonal factor and the elastic matrix element squared, and that the differential cross section can be described by the following formula

$$\mathrm{d}\sigma = \mathrm{d}\sigma_0 \,\frac{\alpha}{2\pi}\,\frac{\mathrm{d}\omega}{\omega}\,\frac{\mathrm{d}\Omega}{(2\pi)}\,\frac{2p_1p_2\,\omega^2}{(p_1k)(p_2k)}. \tag{185}$$

[6] Another popular option is to employ a suitable color basis and the fact that certain color-order ampltudes do not interfere in the limit where number of colors is considered to be a large parameter, see Ref. [28].

It is convenient to denote the scalar products of four-vectors as $p_i p_j = E_i E_j (1 - \cos\theta_{ij}) = E_i E_j \xi_{ij}$, so that the eikonal factor that appears in the formula for the cross section reads

$$\frac{2p_1p_2\ \omega^2}{(p_1k)(p_2k)} = \frac{2\xi_{12}}{\xi_{1k}\xi_{2k}} = 2W(1,2;k). \tag{186}$$

We now re-write the *radiator function* $W(1,2;k)$ in the following way

$$W(1,2;k) = \frac{\xi_{12}}{\xi_{1k}\xi_{2k}} = \frac{1}{2}\left(\frac{\xi_{12}}{\xi_{1k}\xi_{2k}} - \frac{1}{\xi_{2k}} + \frac{1}{\xi_{1k}}\right) + (1 \Leftrightarrow 2) = W_1(1,2;k) + W_2(1,2;k). \tag{187}$$

We would like to interpret the function $W_1(1,2;k)$ as the photon emission off the electron with momentum p_1 and the function $W_2(1,2;k)$ as the photon emission off the positron with momentum p_2. To understand why this interpretation is meaningful, it is useful to study the collinear limits of the two radiator functions. Consider $W_1(1,2;k)$ as an example. If the photon is emitted along the direction of the electron, $\xi_{1,k} \to 0$, $\xi_{2k} \to \xi_{1,2}$ and $W_1(1,2,k) \approx 1/\xi_{1,k} \gg W_2(1,2;k)$. On the contrary, if the photon is emitted along the direction of the positron, $\xi_{2,k} \to 0$, $\xi_{1k} \to \xi_{12}$ and $W_2(1,2;k) \approx 1/\xi_{2,k} \gg W_1(1,2;k)$.

The situation becomes particularly transparent if we integrate over the *azimuthal angle* of the emitted photon defined in the following way. For the function $W_1(1,2;k)$, we choose a reference frame where the electron momentum is the z-axis, i.e. $n_1 = (0,0,1)$, the momentum of the positron is in the $x-z$ plane, i.e. $n_2 = (\sin\theta_{12}, 0, \cos\theta_{12})$ and the photon momentum is arbitrary $\vec{n}_k = (\sin\theta\cos\phi, \sin\theta\sin\phi, \cos\theta)$. Suppose that we want to integrate the function $W_1(1,2;k)$ over the angle ϕ. The only ϕ-dependent scalar product in $W_1(1,2;k)$ is $\xi_{2,k} = 1 - \sin\theta_{12}\sin\theta\cos\phi - \cos\theta_{12}\cos\theta$. The relevant integral reads

$$\int\limits_0^{2\pi} \frac{\mathrm{d}\phi}{(2\pi)} \frac{1}{a + b\cos\phi} = \frac{1}{\sqrt{a^2 - b^2}} \quad \Rightarrow \quad \int\limits_0^{2\pi} \frac{\mathrm{d}\phi}{(2\pi)} \frac{1}{\xi_{2k}} = \frac{1}{|\xi_{1k} - \xi_{12}|}. \tag{188}$$

Using this result to integrate the radiator function W_1, we obtain

$$\int\limits_0^{2\pi} \frac{\mathrm{d}\phi}{(2\pi)} W_1(1,2;k) = \int\limits_0^{2\pi} \frac{\mathrm{d}\phi}{(2\pi)} \frac{1}{2\xi_{1k}} \left(\frac{\xi_{12} - \xi_{1k}}{\xi_{2k}} + 1\right) = \frac{1}{2\xi_{1k}} \left(\frac{\xi_{12} - \xi_{1k}}{|\xi_{12} - \xi_{1k}|} + 1\right) = \frac{\theta(\xi_{12} - \xi_{1k})}{\xi_{1k}}. \tag{189}$$

We repeat the same computation for the second radiator function $W_2(1,2;k)$. However, in this case we integrate over a *different azimuthal angle* since we align the z-axis with the positron direction vector n_2. If we do that, we find

$$\int\limits_0^{2\pi} \frac{\mathrm{d}\phi}{(2\pi)} W_2(1,2;k) = \frac{\theta(\xi_{12} - \xi_{2k})}{\xi_{2k}}. \tag{190}$$

Combining the results for $W_{1,2}$, we obtain a simple formula for the full radiator function

$$W(1,2;k) = W_1(1,2;k) + W_2(1,2;k) \Rightarrow \frac{\theta(\xi_{1k} - \xi_{12})}{\xi_{1k}} + \frac{\theta(\xi_{2k} - \xi_{12})}{\xi_{2k}}. \tag{191}$$

Note that this formula is obtained upon averaging the two contributing radiator functions over *different azimuthal angles*.

We can now use the radiator function Eq. (191) to compute the cross section. We find

$$\mathrm{d}\sigma = \mathrm{d}\sigma_0\ \frac{\alpha}{2\pi}\ \frac{\mathrm{d}\omega}{\omega}\ \sum_{i=1}^{2} \frac{\mathrm{d}\xi_{1k}}{\xi_{1k}} \theta(\xi_{12} - \xi_{ik}). \tag{192}$$

This formula shows remarkable features that enable probabilistic interpretation of soft photon emissions. Indeed, since for small emission angles $\xi_{ij} \approx \theta_{ij}^2/2$, according to Eq. (192), electron and positron emit soft photons independently of each other provided that the emission angle is smaller than the opening angle of the pair, $\theta_{1k} < \theta_{12}$, $\theta_{2k} < \theta_{12}$. If emission at a larger angle happens, the *interference* of emissions by the electron and the positron effectively shuts off the radiation completely.

What makes this result interesting for the construction of a parton shower is that it appears to be possible to describe soft emissions by making *educated choices of evolution variables*. Indeed, we have so far discussed the parton shower evolution as being driven by the logarithmic integration over the transverse momentum of the emitted particle. However, since $k_\perp \sim \omega\theta$, one can trade logarithmic integration over the transverse momentum for the integration over emission angle

$$\frac{\mathrm{d}k_\perp}{k_\perp} = \frac{\mathrm{d}\theta}{\theta} = \frac{1}{2}\,\frac{\mathrm{d}\xi}{\xi} \tag{193}$$

The natural ordering of the emission angles, i.e. larger emission angles closer to a hard process followed by smaller emission angles at the end of the cascade, allows to resum both *soft* and *collinear* logarithms in an event.

Although the above discussion is sufficiently general to be used in QCD parton showers, there is one aspect of it that is too QED-specific and, for this reason, warrants a clarification. Indeed, in QED, the variety of charge-changing processes is very limited since in a splitting $a \to b + c$, one of the particles is always neutral. This is clearly not the case in QCD, where a color-charged gluon can split into a quark-anti-quark pair. Since working with QCD amplitudes and introducing convenient notations for color charges will take us astray, it is more useful to introduce a toy model that, on one hand, will be easy to work with and, on the other hand, will not suffer from the limitation of QED described above. To this end, we consider a soft photon emission amplitude off a final state with three charged particles

$$\mathcal{M} \sim \sum_{i=1}^{3} Q_i \frac{p_i\epsilon}{p_i k}\mathcal{M}_0. \tag{194}$$

Gauge-invariance dictates that $\sum\limits_{i=1}^{3} Q_i = 0$, but does not impose constraints on individual charges. Upon squaring the amplitude and summing over photon polarizations, we find

$$|\mathcal{M}|^2 \sim -\sum_{ij} Q_i Q_j \frac{p_i p_j}{(p_i k)(p_j k)}\,|\mathcal{M}_0|^2. \tag{195}$$

Expressing this result in terms of the radiator function, we obtain

$$W = -Q_1Q_2W_{12} - Q_1Q_3W_{13} - Q_2Q_3W_{23}. \tag{196}$$

We then re-write charge products through charge squares, e.g. $-Q_1Q_2 = (Q_1^2 + Q_2^2 - Q_3^2)/2$ using $Q_1 + Q_2 + Q_3 = 0$ and derive

$$W = \frac{1}{2}\Big[Q_1^2\,(W_{12} + W_{13} - W_{23}) + Q_2^2\,(W_{12} + W_{23} - W_{13}) + Q_3^2\,(W_{13} + W_{23} - W_{12})\Big]. \tag{197}$$

We would like to re-write this expression in a way that will make an interpretation in terms of successive independent emissions possible. To this end, we split each radiator function into a sum of relevant terms and average each such term over respective azimuthal angles. We also consider a kinematic configuration where the opening angle between p_1 and p_2 is much smaller than the opening angle between p_{12} and p_3, c.f. Fig. 9.

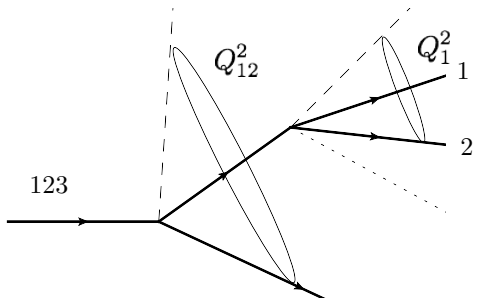

Fig. 9: Soft emissions after azimuthal ordering, see Eq. (202).

To see how the hierarchy of angles can be exploited, consider the term in Eq. (197) that is proportional to Q_1^2 and write

$$\begin{aligned} &W_{12}+W_{13}-W_{23}\to W_{12}^{[1]}+W_{12}^{[2]}+W_{13}^{[1]}+W_{13}^{[3]}-W_{23}^{[2]}-W_{23}^{[3]}\\ &=2W_{12}^{[1]}+\left\{(W_{13}^{[1]}-W_{12}^{[1]})+(W_{12}^{[1]}-W_{23}^{[2]})\right\}+\left\{W_{13}^{[3]}-W_{23}^{[3]}\right\}. \end{aligned} \tag{198}$$

We now study the different terms separately. We find

$$\begin{aligned} (W_{13}^{[1]}-W_{12}^{[1]})+(W_{12}^{[1]}-W_{23}^{[2]})&=\frac{(\theta(\xi_{13}-\xi_{1k})-\theta(\xi_{12}-\xi_{1k}))}{\xi_{1k}}-\frac{(\theta(\xi_{23}-\xi_{2k})-\theta(\xi_{12}-\xi_{2k}))}{\xi_{2k}}\\ &\Rightarrow\int \mathrm{d}\Omega_k\left[(W_{13}^{[1]}-W_{12}^{[1]})+(W_{12}^{[1]}-W_{23}^{[2]})\right]=\ln\frac{\theta_{13}}{\theta_{23}}\sim 1, \end{aligned} \tag{199}$$

for $\theta_{12}\ll\theta_{13}$. This result implies that the combination of radiator functions displayed in Eq. (199) *does not* lead to large logarithmic corrections and, for this reason, can be neglected. A similar analysis of the last term in Eq. (198) leads to a similar conclusion

$$(W_{13}^{[3]}-W_{23}^{[3]})=\frac{\theta(\xi_{13}-\xi_{3k})}{\xi_{3k}}-\frac{\theta(\xi_{23}-\xi_{3k})}{\xi_{3k}}\Rightarrow\int \mathrm{d}\Omega_k(W_{13}^{[3]}-W_{23}^{[3]})=\ln\frac{\theta_{13}}{\theta_{23}}\sim 1. \tag{200}$$

Hence, for the kinematic case that we are interested in, the following replacement is valid with the logarithmic accuracy

$$W_{12}+W_{13}-W_{23}\to 2W_{12}. \tag{201}$$

Similar arguments allow us to simplify the radiator function in Eq. (197) and write it as

$$W\approx Q_1^2W_{12}^{[1]}+Q_2^2W_{12}^{[2]}+(Q_1+Q_2)^2W_{12,3}^{[12]}+Q_3^2W_{12,3}^{[3]}. \tag{202}$$

Here $W_{12,3}^{[12]}$ describes emission off the "parent parton" of the two partons 1 and 2. It reads $W_{12,3}^{[12]}=\theta(\xi_{12,3}-\xi_{12,k})\theta(\xi_{12,k}-\xi_{12})/\xi_{12,k}$.

The interpretation of Eq. (202) is straightforward. It shows that soft radiation can be described by independent emissions off *four* particles that appear in the amplitude – partons $1,2$ and 3 and the "parent" of the two partons 1 and 2. The radiation off each of these particles is proportional to its charge squared. The radiation is restricted by the opening angles of the corresponding "dipoles". For example, the "parent" of 1 and 2 radiates to an opening angle between $\vec{n}_1\sim\vec{n}_2$ an $\vec{n}_3$ but 1 and 2 radiate into an opening angle between themselves. It should be clear from previous discussions that this structure easily lends itself to a parton shower description provided that opening angles are chosen as independent evolution variables.

7.4 Parton showers connect perturbative and non-perturbative descriptions of hadron collisions

We have seen that parton showers can be used to generate unweighted events and, within certain approximations, produce final states with arbitrary number of quarks and gluons starting from a few energetic particles in the event. These initial hard particles provide seeds of energy flows that a hardly affected by non-perturbative effects. These energy flows provide foundations for hadron jets, a trademark of high-energy collisions. Collinear and soft radiation described by parton showers builds up these jets and fills them with large number of partons. When relative transverse momenta of gluons and quarks generated by parton showers become small, QCD turns into a non-perturbative theory and generation of further emissions of quarks and gluons becomes meaningless. At this point, one employs phenomenological models that describe a parton-to-hadron transition, i.e. they allow us to transform an ensemble of quarks and gluons into a *hadronic* final state. Although the description of such a transition is empirical (see e.g. Refs. [7, 26]), it is very important since hadrons, not partons, hit particle detectors. Therefore, properties of hard events that we strive to understand are deduced from particle composition, multiplicities and energy depositions of hadrons observed in particle detectors. Our ability to connect these measurements with properties of the hard scattering relies on parton shower Monte Carlo and the description of parton-to-hadron transition.

It is important to stress that the interplay between fixed orders and parton showers drives the development of both tools. In particular, spectacular progress in our ability to perform sophisticated fixed order computations lead to a possibility to describe better the kinematics of *hard* jets, as produced in short-distance collisions, leaving the parton shower with a task that it does best – filling these jets with the soft and collinear radiation. The ideas of *merging* and *matching* [27] emphasize the need to combine fixed orders with parton showers; they also put additional pressure on parton shower algorithms to become more refined theoretical tools with higher (and well-defined) parametric accuracy. The progress in this field will be crucial for extracting maximal physics information from the LHC and making precision physics at the LHC a viable opportunity.

8 Conclusions

The goal of these lectures was to describe how the theory of strong interactions – Quantum Chromodynamics – is applied to describe hard collisions at the LHC. QCD is crucial for the success of the LHC physics program since two strongly interacting particles – protons – are collided there. In spite of this fact, if we look at the right observables, LHC physics is mainly determined by interactions of quarks and gluons rather than hadrons and these interactions can be understood directly from the Standard Model Lagrangian. Recent theoretical developments that include advances in fixed order computations, resummations, parton shower algorithms and determination of parton distribution functions allowed us to describe hard scattering data at the LHC with very high precision. We hope that this high precision predictions for many LHC observabels will, one day, be used to find something unexpected and will, in this way, completement direct searches for physics beyond the Standard Model at the LHC [29].

Acknowledgments

I would like to thank the organizers of the CERN-JINR Summer School for an opportunity to present these lectures and for an excellent organization. I am grateful to students for their interest and active participation in lectures and in the discussion sessions.

References

[1] ATLAS collaboration, *Observation of a new particle in the search for the Standard Model Higgs boson with the ATLAS detector at the LHC*, Phys. Lett. B **716** (2012) 1.

[2] CMS collaboration, *Observation of a new boson at a mass of 125 GeV with the CMS experiment at the LHC*, Phys. Lett. B **716** (2012) 30.

[3] J.C. Collins, D.E. Soper and G. Sterman, in *Perturbative Quantum Chromodynamics*, ed. A. H. Mueller (World Scientific, Singapore, 1989), p.1; J. C. Collins and D. E. Soper, *The Theorems of Perturbative QCD*, Ann. Rev. Nucl. Part. Sci. **37** (1987) 383.

[4] G. P. Salam, *Towards Jetography*, Eur. Phys. J. C **67** (2010) 637.

[5] M. E. Peskin and D. V. Schroeder, *An Introduction to quantum field theory*, Westview Press, 1995.

[6] M. D. Schwartz, *Quantum Field Theory and the Standard Model*, Cambridge University Press, 2014.

[7] R.K. Ellis, W.J. Stirling and B.R. Webber, *QCD and collider physics*, Cambridge Monographs on Particle Physics, Nuclear Physics and Cosmology, 1996.

[8] Yu.L. Dokshitzer, V.A. Khoze, A.H. Mueller and S.I. Troyan, *Basics of Perturbative QCD*, Editions Frontieres, 1991.

[9] G. Dissertori, I. Knowles, M. Schmelling, *Quantum Chromodynamics*, Oxford Science Publications, 2009.

[10] S. Catani and M. H. Seymour, *A General algorithm for calculating jet cross-sections in NLO QCD*, Nucl. Phys. B **485** (1997) 291; Erratum: [Nucl. Phys. B **510** (1998) 503].

[11] S. Frixione, Z. Kunszt and A. Signer, *Three jet cross-sections to next-to-leading order*, Nucl. Phys. B **467** (1996) 399.

[12] G. Ossola, C. G. Papadopoulos and R. Pittau, *'Reducing full one-loop amplitudes to scalar integrals at the integrand level*, Nucl. Phys. B **763** (2007) 147.

[13] C. F. Berger, Z. Bern, L. J. Dixon, F. Febres Cordero, D. Forde, H. Ita, D. A. Kosower and D. Maitre, *An Automated Implementation of On-Shell Methods for One-Loop Amplitudes*, Phys. Rev. D **78** (2008) 036003; R. K. Ellis, W. T. Giele and Z. Kunszt, *A Numerical Unitarity Formalism for Evaluating One-Loop Amplitudes* JHEP **0803** (2008) 003; W. T. Giele, Z. Kunszt and K. Melnikov, *Full one-loop amplitudes from tree amplitudes*, JHEP **0804** (2008) 049.

[14] S. Catani and M. Grazzini, *An NNLO subtraction formalism in hadron collisions and its application to Higgs boson production at the LHC*, Phys. Rev. Lett. **98** (2007) 222002; R. Boughezal, C. Focke, X. Liu and F. Petriello, *W-boson production in association with a jet at next-to-next-to-leading order in perturbative QCD*, Phys. Rev. Lett. **115** (2015) 062002; J. Gaunt, M. Stahlhofen, F. J. Tackmann and J. R. Walsh, *N-jettiness Subtractions for NNLO QCD Calculations*, JHEP **1509** (2015) 058; A. Gehrmann-De Ridder, T. Gehrmann and E. W. N. Glover, *Antenna subtraction at NNLO*, JHEP **0509** (2005) 056 E. W. Nigel Glover and J. Pires, *Antenna subtraction for gluon scattering at NNLO*, JHEP **1006**, 096 (2010) M. Czakon, *Double-real radiation in hadronic top quark pair production as a proof of a certain concept*, Nucl. Phys. B **849** (2011), 250; M. Czakon and D. Heymes, *Four-dimensional formulation of the sector-improved residue subtraction scheme*, Nucl. Phys. B **890** (2014) 152; F. Caola, K. Melnikov and R. Röntsch, *Nested soft-collinear subtractions in NNLO QCD computations*, Eur. Phys. J. C **77**, (2017) 248;

[15] See e.g. T. Gehrmann, M. Grazzini, S. Kallweit, P. Maierhöfer, A. von Manteuffel, S. Pozzorini, D. Rathlev and L. Tancredi, *W^+W^- Production at Hadron Colliders in Next to Next to Leading Order QCD*, Phys. Rev. Lett. **113**, no. 21, 212001 (2014); R. Boughezal, F. Caola, K. Melnikov, F. Petriello and M. Schulze, *Higgs boson production in association with a jet at next-to-next-to-leading order*, Phys. Rev. Lett. **115** (2015) 082003; M. Czakon, D. Heymes and A. Mitov, *High-precision differential predictions for top-quark pairs at the LHC* Phys. Rev. Lett. **116** (2016) 082003; J. Currie, A. Gehrmann-De Ridder, T. Gehrmann, E. W. N. Glover, A. Huss and J. Pires, *Precise predictions for dijet production at the LHC*, Phys. Rev. Lett. **119** (2017) 152001; A. Gehrmann-De Ridder, T. Gehrmann, E. W. N. Glover, A. Huss and T. A. Morgan, *Precise QCD predictions for the production of a Z boson in association with a hadronic jet*, Phys. Rev. Lett. **117**, no. 2, 022001 (2016); E. L. Berger, J. Gao, C.-P. Yuan and H. X. Zhu, *NNLO QCD Corrections to t-channel Single Top-Quark Production and Decay*, Phys. Rev. D **94** (2016) no.7, 071501.

[16] C. G. Bollini and J. J. Giambiagi, *Dimensional Renormalization: The Number of Dimensions as a Regularizing Parameter,* Nuovo Cim. B **12** (1972) 20.

[17] S. Catani, *The Singular behavior of QCD amplitudes at two loop order*, Phys. Lett. B **427** (1998) 161.

[18] V. N. Gribov and L. N. Lipatov, *Deep inelastic e p scattering in perturbation theory*, Sov. J. Nucl. Phys. **15** (1972) 438;

[19] Y. L. Dokshitzer, *Calculation of the Structure Functions for Deep Inelastic Scattering and e+ e- Annihilation by Perturbation Theory in Quantum Chromodynamics*, Sov. Phys. JETP **46** (1977) 641; G. Altarelli and G. Parisi, *Asymptotic Freedom in Parton Language*, Nucl. Phys. B **126** (1977) 298.

[20] G. Bozzi, S. Catani, G. Ferrera, D. de Florian and M. Grazzini, Phys. Lett. B **696** (2011) 207.

[21] G. Parisi and R. Petronzio, *Small Transverse Momentum Distributions in Hard Processes*, Nucl. Phys. B **154** (1979) 279.

[22] G. Luisoni and S. Marzani, *QCD resummation for hadronic final states,* J. Phys. G **42** (2015) 103101.

[23] M. Abramowitz and I. Stegun, *Handbook of Mathematical Functions*, NBS, 1964.

[24] J. C. Collins, D. E. Soper and G. F. Sterman, *Transverse Momentum Distribution in Drell-Yan Pair and W and Z Boson Production*, Nucl. Phys. B **250** (1985) 199.

[25] J. Butterworth *et al.*, *PDF4LHC recommendations for LHC Run II*, J. Phys. G **43** (2016) 023001; A. Accardi *et al.*, *A Critical Appraisal and Evaluation of Modern PDFs*, Eur. Phys. J. C **76** (2016) 471.

[26] A. Buckley *et al.*, *General-purpose event generators for LHC physics*, Phys. Rept. **504** (2011) 145.

[27] S. Catani, F. Krauss, R. Kuhn and B. R. Webber, *QCD matrix elements + parton showers*, JHEP **0111** (2001) 063; S. Frixione and B. R. Webber, *Matching NLO QCD computations and parton shower simulations*, JHEP **0206** (2002) 029; S. Frixione, P. Nason and C. Oleari, *Matching NLO QCD computations with Parton Shower simulations: the POWHEG method*, JHEP **0711** (2007) 070; S. Alioli, C. W. Bauer, C. J. Berggren, A. Hornig, F. J. Tackmann, C. K. Vermilion, J. R. Walsh and S. Zuberi, *Combining Higher-Order Resummation with Multiple NLO Calculations and Parton Showers in GENEVA*, JHEP **1309** (2013) 120.

[28] S. Plätzer, *Summing Large-N Towers in Colour Flow Evolution*, Eur. Phys. J. C **74** (2014) 2907.

[29] S. Alioli, M. Farina, D. Pappadopulo and J. T. Ruderman, *Catching a New Force by the Tail*, arXiv:1712.02347 [hep-ph]; C. Frye, M. Freytsis, J. Scholtz and M. J. Strassler, *Precision Diboson Observables for the LHC*, JHEP **1603** (2016) 171; A. Azatov, C. Grojean, A. Paul and E. Salvioni, *Resolving gluon fusion loops at current and future hadron colliders*, JHEP **1609** (2016) 123.